NASA TECHNICAL NOTE

NASA TN D-5930

NASA TN D-5930

AN EXPERIMENTAL STUDY OF A CARBON-PHENOLIC ABLATION MATERIAL

by Kenneth Sutton

Langley Research Center
Hampton, Va. 23365

NATIONAL AERONAUTICS AND SPACE ADMINISTRATION • WASHINGTON, D. C. • SEPTEMBER 1970

1. Report No.
NASA TN D-5930

2. Government Accession No.

3. Recipient's Catalog No.

4. Title and Subtitle
AN EXPERIMENTAL STUDY OF A CARBON-PHENOLIC ABLATION MATERIAL

5. Report Date
September 1970

6. Performing Organization Code

7. Author(s)
Kenneth Sutton

8. Performing Organization Report No.
L-6455

9. Performing Organization Name and Address
NASA Langley Research Center
Hampton, Va. 23365

10. Work Unit No.
124-07-18-06

11. Contract or Grant No.

12. Sponsoring Agency Name and Address
National Aeronautics and Space Administration
Washington, D.C. 20546

13. Type of Report and Period Covered
Technical Note

14. Sponsoring Agency Code

15. Supplementary Notes

16. Abstract

The experimental results from a ground-test program are presented for a carbon-phenolic heat-shield material designated Narmco 4028. The tests were conducted in supersonic streams of air, nitrogen, and air-nitrogen mixtures at model stagnation pressures from 0.07 to 11 atmospheres (1 atmosphere equals 101.325 kN/m^2) and stagnation enthalpies from 1100 to 11 000 Btu/lbm (2.55 to 25.50 MJ/kg). Mechanical char removal of the material did not occur in the nitrogen tests but did occur in air and air-nitrogen mixtures at pressures as low as 2.4 atmospheres depending upon the oxygen mass fraction in the stream. The experimental results were compared with predictions from an ablation computer program.

17. Key Words (Suggested by Author(s))
Ablation
Carbon-phenolic material
Heat shield

18. Distribution Statement
Unclassified – Unlimited

19. Security Classif. (of this report)
Unclassified

20. Security Classif. (of this page)
Unclassified

21. No. of Pages
51

22. Price*
$3.00

*For sale by the Clearinghouse for Federal Scientific and Technical Information
Springfield, Virginia 22151

AN EXPERIMENTAL STUDY OF A CARBON-PHENOLIC ABLATION MATERIAL

By Kenneth Sutton
Langley Research Center

SUMMARY

An experimental ground-test program was conducted to evaluate the ablative characteristics of a carbon-phenolic heat-shield material designated Narmco 4028. The experimental results were compared with predictions from an ablation computer program. Tests were also conducted to evaluate the effects of hole patterns in the material and the effects of injecting water into the flow field through holes in the material. These latter tests were in support of a flight project called project RAM (radio attenuation measurements). The test facilities used in the investigation were the Langley 11-inch ceramic-heated tunnel and the Langley 20-inch hypersonic arc-heated tunnel.

In the present tests, mechanical char removal of the material occurred for tests in air at model stagnation pressure above 2.4 atmospheres, but did not occur in nitrogen for pressures up to 11 atmospheres (1 atmosphere equals 101.325 kN/m^2). The mechanical char removal did not remove the entire char layer. An expansion of the material which can offset chemical removal also occurred, and there was an effect of fiber orientation. The experimental data showed that holes in the material can survive without enlargement and maintain their integrity. Water injected into the flow field through holes in the material had no significant effects on the behavior of the material and the holes remained free of any restrictions to the water flow during the tests.

The computer program used in the study was successful in predicting gross trends in material behavior. However, there was scatter in the comparisons between experimental and computer results which is attributed to phenomena, such as mechanical char removal, material expansion, and material degradation during cooldown, which could not be accounted for in the computer program.

INTRODUCTION

An experimental ground-test study was undertaken to evaluate the ablative characteristics of a carbon-phenolic heat-shield material. The material studied is designated Narmco 4028, a composite of 50 percent by weight of carbon fibers and 50-percent phenolic resin. The purpose of the present study was twofold.

First, the Langley Research Center has a continuing program of ground-test studies to investigate various types of ablators for possible use as heat shields for reentry flight application. Also, the experimental results are used to evaluate the ability of analytical computer programs to predict the ablative response of various materials. For this objective, models of Narmco 4028 material were tested in ground facilities over a range of aerodynamic conditions to obtain experimental results of char recession, thermal degradation of virgin material, char retention, back-surface temperature rise, surface temperature, fiber orientation effects, and observation of possible peculiarities of the material. The experimental results were compared with analytical computer predictions.

Second, the Narmco 4028 material is used as the heat shield at the nose region for some of the reentry flight vehicles in the project RAM (radio attenuation measurement) series at the Langley Research Center. Project RAM is investigating the blackout phenomena of radio communications encountered during atmospheric reentry and makes extensive use of flight vehicles to obtain experimental data. (See refs. 1, 2, and 3.) The requirements of the flight experiment imposed a unique feature for this heat shield. Water is injected through patterns of holes in the Narmco 4028 material into the flow field during the flight experiment. The results from the present study were part of the flight verification of the Narmco 4028 material for the RAM series. In addition to the necessity of knowing the general ablative behavior of Narmco 4028, tests were conducted to study the effects of holes in the material and the effects of water injection on the ablative behavior of the material. A full-scale replica of the RAM heat shield was tested in a rocket-engine exhaust as additional flight verification and the results of that test have previously been published in reference 4.

The test facilities used in the present study were the Langley 11-inch ceramic-heated tunnel and the Langley 20-inch hypersonic arc-heated tunnel. The range of stagnation enthalpy was 1100 to 11 000 Btu/lbm (2.55 to 25.50 MJ/kg) and the range of model stagnation pressure was from 0.07 to 11 atmospheres. Stagnation heating rates were obtained from 130 to 1600 Btu/ft^2-sec (1.48 to 18.20 MW/m^2). These ranges are for each parameter and are not inclusive of the other parameters.

SYMBOLS

The units used for the physical quantities defined in this paper are given both in the U.S. Customary Units and in the International System of Units (SI). (See ref. 5.)

H_s stagnation enthalpy, Btu/lbm (MJ/kg)

K_o mass fraction of oxygen in test stream

l	length of test model, in. (cm)
M_O	total cold-wall oxygen mass flux, $\frac{\dot{q}_s K_O t}{H_s}$, lbm/ft^2 (kg/m^2)
p_s	stagnation-point pressure, atm
$\dot{q}_s$	stagnation-point cold-wall heating rate, Btu/ft^2-sec (MW/m^2)
T_s	approximate equilibrium stagnation-point surface temperature, $^{\circ}$R (K)
t	time, sec (s)
$\dot{w}$	flow rate of injected water, lbm/sec (kg/s)
x_c	char thickness, in. (cm)

Primed symbols refer to computer results.

TEST FACILITIES

The test facilities used in the present investigation were the Langley 11-inch ceramic-heated tunnel and the Langley 20-inch hypersonic arc-heated tunnel. In figure 1, the approximate test conditions for a 1-inch-diameter (2.54-cm) hemispherical model are shown. Tests using air, nitrogen, and air-nitrogen mixtures as the test environment were conducted. The test conditions for the individual tests are given in tables I to IV.

The Langley 11-inch ceramic-heated tunnel was used for the test at higher pressures (6 to 11 atmospheres) although the facility has a low enthalpy capability. In this facility the test gas is heated by flowing through a pebble-bed heat exchanger before expanding through the nozzle. A free-jet Mach 2 nozzle with a 1.33-inch-diameter (3.38-cm) exit was used for the tests. The description and operating conditions of this facility with the Mach 2 nozzle is given in reference 6.

A wider range of test conditions and higher enthalpies could be obtained in the Langley 20-inch hypersonic arc-heated tunnel. The maximum model stagnation pressure in this facility is 3 atmospheres. This facility uses a rotating, radial, dc electric arc to heat the test gas. Three separate nozzles with exit diameters of 2.0, 3.3, and 6.6 inches (5.08, 8.38, and 16.76 cm) were used for this study. A description of this facility is given in reference 7.

MATERIAL AND MODEL DESCRIPTION

Narmco 4028 is a composite material of 50 percent by weight of phenolic resin and 50 percent of 1/4-inch (0.63-cm) carbon fibers. The nominal density of the virgin material is 87 lbm/ft^3 (1392 kg/m^3). An elemental chemical analysis for the nondegraded material is given in table V. As part of the present study, steady-state measurements of the thermal properties of the nondegraded and charred material were performed under contract. These results are given in reference 8.

The molding and curing of the commercially supplied molding compound were performed by the Langley Research Center. The size of the molded billets was approximately 12 inches (30.48 cm) in diameter and 4 inches (10.16 cm) thick. The carbon fibers will have a preferred orientation depending on method of molding. This preferred orientation has been noted in reference 9 for similar carbon and graphite composite materials. In the present billets the length of the fibers were alined perpendicular to the direction of the applied pressure during the molding operation. This fiber alinement is illustrated by the sketch in figure 2.

Several model designs were used in the present investigation. Most of the models were machined from the molded billets described. The models shown in figure 3 were used to study the general behavior of the material and its char. For each nose shape, models were made so that the carbon fibers were alined both perpendicular and parallel to the direction of the free-stream flow during the tests.

The effect of fiber orientation was further investigated by the use of the model design shown in figure 4. The test specimen of Narmco 4028 was bonded to a shell made of mild steel. (See fig. 4(a).) Models of this design were made, with orientation of the fibers in the test specimen being perpendicular, parallel, and shingled with respect to the flow of the test stream. (See fig. 4(b).) A special mold and molding technique was used to obtain the shingled orientation of fibers.

The hemispherical models with perpendicular-fiber orientation shown in figure 3(a) were used to investigate the effect of holes in the material. Holes were drilled in the models in three patterns as shown by the photographs in figure 5. The holes in the 1-hole pattern and the 4-hole pattern were 0.06 inch (0.15 cm) in diameter; whereas, the holes in the 13-hole pattern were 0.03 inch (0.08 cm) in diameter. The depth of the holes in all three patterns was approximately 0.6 inch (1.5 cm).

The model design shown in figure 6 was used for the tests of the effects of water injection. The test specimen had shingled-fiber orientation (fig. 4(b)) and was bonded to a mild steel holder with passages for the injection of water. Holes with diameters of 0.046 inch (0.117 cm) were located at the stagnation point and at 60° and 81° from the

stagnation point. As shown in figure 6(a), only the stagnation-point holes were connected to the water passage for the models used to study stagnation-point injection. For side injection, both the 60° and 81° holes were connected to the water passage. (See fig. 6(b).)

The model design shown in figure 7 was used in the measurement of back-surface temperature rise for the material. The test specimens (fig. 7(a)) were machined from the molded billets with both perpendicular- and parallel-fiber orientation. As shown in the assembly drawing (fig. 7(b)), a calorimetric plate of 1/64-inch-thick (0.04-cm) copper with three 30-gage chromel-alumel thermocouples is bonded to the back surface of the test specimen. The nose assembly is bonded to a cylindrical steel holder protected with a phenolic-cork composite. At the more severe test conditions, the cylindrical sidewalls were further protected by wrapping with fiber-glass tape. Reference 10 used this model design for similar tests.

TEST PROCEDURE AND INSTRUMENTATION

The test procedure was basically the same for all models in each of the two facilities. The test environment would be set by standard facility procedure; after the equilibrium stream condition was obtained, the model would be inserted into the test stream for the particular exposure time. At the end of exposure time the model would be retracted from the stream. For the tests in the ceramic-heated tunnel, a stream of argon was sprayed over the model to quench flaming of the model after retraction from the test stream.

The length of the test specimen was measured before and after the test. The specimens were sectioned after testing for further study; the studies included measurement of the depth of degradation of the material (that is char thickness).

The response of the model thermocouples was recorded on an oscillograph. Surface temperature of the model was measured with a photographic pyrometer. This type of instrument is described in reference 11; however, a more advanced photographic pyrometer than those described in reference 11 was used in the present tests and the temperature range of this type of instrument has been extended to 7000° R (3900 K). Motion-picture cameras with speeds up to 400 frames per second were used to record the behavior of the models during a test. The models could also be visually observed during a test.

The stagnation enthalpies and stagnation pressures for the tests in the ceramic-heated tunnel were taken from the results of reference 6. The heating rates were calculated by using these parameters and the heating-rate equations of reference 12. The oxygen mass fractions were measured with a calibrated choked orifice system used to mix the air and nitrogen. For the tests in the hypersonic arc-heated tunnel, the heating rates and stagnation pressures were measured with thin-wall calorimeters and pressure probes

respectively. These parameters were then used to calculate the stagnation enthalpies by the heating-rate equations of reference 12. The oxygen mass fractions were calculated from a known volumetric mixing of air and nitrogen.

For the water-injection tests, an instrumentation console was used which incorporated all the instruments necessary to control and record the water injection rates properly. The source of the water supply was a container filled with water and pressurized by air.

RESULTS AND DISCUSSION

The results of the individual tests are given in tables I to IV. In these tables are listed the stagnation-point length change, the char thickness, and the approximate equilibrium, stagnation point, surface temperature of the models for each test condition. For the model length change, a negative sign (-) refers to a recession of the model and a positive sign (+) refers to an expansion of the model. The char thicknesses are only given for those cases where the thermal degradation of the virgin material could be attributed to one-dimensional heat conduction.

Mechanical Char Removal

Mechanical char removal of the material was observed to occur at certain test conditions for air and air-nitrogen mixtures but not in nitrogen as noted in the result tables. This mechanical char removal is defined as pieces of char being removed from the char surface. For the tests in which mechanical char removal occurred, pieces of char would be observed leaving the surface of the model and the models did not retain a smooth char surface. The observation of mechanical char removal was made visually both during the tests and from the motion-picture films of the tests. The mechanical char removal of some representative tests is shown in figure 8 by photographs taken from the motion-picture films.

The regime of mechanical char removal is shown by the data in figure 9 and photographs in figure 10. These data are for the model designs shown in figure 3 with perpendicular-fiber orientation. Mechanical char removal did not occur in nitrogen over the entire test range nor in air and air-nitrogen mixtures at stagnation pressures below 2 atmospheres. At stagnation pressures greater than 6 atmospheres, mechanical char removal occurred whenever oxygen was present in the test stream. For air environments ($K_O = 0.23$), mechanical char removal occurred at stagnation pressures as low as 2.4 atmospheres.

The mechanical char removal for the material is a surface phenomenon and the entire char layer is not removed. Photographs of sectioned models are shown in

figure 11. As can be seen from the photographs, there is a thick char layer present even though severe mechanical char removal had occurred.

The cause of the mechanical char removal was not determined in the present tests. Char removal by aerodynamic shear is one possible mechanism. However, tests in nitrogen at stagnation pressures as high as 11 atmospheres and aerodynamic shears of 62 lbf/ft^2 (2.97 kN/m^2) did not show any mechanical char removal. Mechanical char removal did occur at these test conditions in air and in air-nitrogen mixtures. Therefore, aerodynamic shear by itself is not considered the cause of the removal. In reference 13 is presented a theory for multidimensional gas flow through permeable char layers and this theory shows that an inflow of gas from the boundary layer into the char layer is possible. The inflow of a gas containing oxygen could oxidize and weaken the interior structure of the char to such an extent that mechanical char removal by aerodynamic shear is then possible. The present tests had the favorable conditions of small models, high pressures, and thick char layers for gas inflow as presented in reference 13. This concept of a weakening of the char due to gas inflow is only suggested as a possible mechanism and was not proven in present tests. However, the presence of oxygen has a definite influence on the initiation of the char removal.

Recession-Rate Data

Good recession-rate data for chemical removal of the char were not obtained in the present tests. At the higher pressure conditions the mechanical char removal was superimposed on the chemical removal. Also, over the entire range of test conditions, there was a measurable expansion of the material which offset recession. In many of the tests, the length of the model was greater after the test than before the test. This expansion of the material occurred for all model designs. An attempt to correlate the expansion with various parameters was unsuccessful. Because of this mechanical removal and material expansion, a good experimental comparison could not be made with chemical-removal theories for the char even though the model surface temperatures were in the range usually associated with diffusion-controlled oxidation and sublimation of the char.

Fiber Orientation

The direction of the orientation of the carbon fibers with respect to the test stream flow has an effect on the ablative behavior of the material. In figure 12 are shown photographs of representative models after testing with fiber orientation perpendicular and parallel to the free-stream flow. Crevices are formed in the char layer at the nose region of the models with parallel-fiber orientation. This effect was not noted for any of the perpendicular-fiber models. Also, the recessions of the models with parallel-fiber orientation were always greater than those of the perpendicular-fiber models for

comparable test environments. In figure 13 is shown the comparison of stagnation-point length change between parallel and perpendicular fibers at comparable test conditions.

The model design shown in figure 4 was used to study further the effect of fiber orientation. In figure 14 representative models with the three different fiber orientations are shown. Again, crevices are formed at the nose region of the models with parallel-fiber orientation. No crevices were formed for the models with perpendicular- or shingled-fiber orientation. Also, the perpendicular- and shingled-fiber models have the same general response to an environment. There was no apparent mechanical char removal along the sidewalls of the models in any of the tests, regardless of the type of fiber orientation.

The crevices formed in the char layer for the parallel-fiber orientation do not extend into the nondegraded material. Even the most severe crevices did not extend past the pyrolysis interface. Also, the pyrolysis interfaces for these models have the same contour as the general contour of the exterior surface of the model.

Hole Patterns

The effect of holes in the material was studied at both high- and low-pressure conditions. No enlargements of the holes occurred in any of the tests as illustrated by the photographs in figure 15 for the highest pressure test condition and for severe mechanical char removal. The present experimental results indicate that holes can survive and maintain their integrity in the Narmco 4028 material.

At test conditions where models without holes did not have any mechanical char removal, the models with hole patterns also did not indicate any mechanical char removal. In the test regime for mechanical char removal, there is an effect of hole pattern on the stagnation recession of the models. In figure 16 the stagnation-point recession is shown for models with hole patterns tested at the highest pressure condition. At the longer test times there is greater recession for the models with hole patterns of 4 and 13 holes. The holes for the 4-hole model were located at the region of maximum shear.

Water Injection

The effect of water injection on the behavior of the Narmco 4028 material was investigated at both a high-pressure and a low-pressure test condition. In these tests the water was injected into the flow field either from an orifice at the stagnation point of the model (stagnation-point injection) or from two orifices at 60° and 81° from the stagnation point of the model (sidewall injection). The initiation of water injection was only after the model had reached a high surface temperature. The water was then

injected in pulses of 0.2 second on and 0.3 second off for the duration of the test. During the RAM flight experiments the water will also be injected in pulses. The flow rates of the injected water for each test are given in table III. Photographs of representative models during the test and after testing are shown in figures 17, 18, and 19. The stagnation-point surface temperatures were 4100° R (2278 K) for the models tested at the high-pressure condition and 5300° R (2944 K) for the low-pressure condition. Therefore, the models had a high surface temperature for any possible reaction with the water. For stagnation-point injection, the stagnation region of the model was cooled to a much lower temperature during the injection pulse, but the temperature was regained between the water pulses.

The basic behavior of the material for the water-injection tests was approximately the same as that for the tests without injection at comparable test conditions. The water injection neither increased nor decreased the effects of mechanical char removal. The stagnation-point length changes of the water-injection models were comparable with those obtained for the models without injection. Also, the holes in the material remained free of any restrictions to the water flow during the tests and the holes were clear after the tests.

Crack Formation

Another feature observed in the present tests was the formation of cracks in the virgin material for the model design shown in figure 3. The cracks developed only in the models with perpendicular-fiber orientation. Examples of these cracks are shown in figure 11. The cracks did not always extend to the exterior surface of the models. The models constructed with thinner material (figs. 4, 6, and 7) did not show any cracks.

Model Flaming

As previously noted in the section "Test Procedure and Instrumentation," a stream of argon was sprayed over the models to quench flaming of the model after retraction from the test stream for the tests in the ceramic-heated tunnel. Preliminary tests showed severe flaming due to combustion of pyrolysis gases (from continued degradation of the virgin material) with the atmospheric environment. A photograph taken from motion-picture film of a preliminary test is shown in figure 20 and illustrates the degree of flaming that would continue from 3 to 5 minutes after model retraction from the stream. The spraying with argon stopped this flaming during the actual test program.

Comparison with Computer Predictions

A study was made of the comparison between the experimental results and the predicted results from an ablation computer program. A description of the computer

program is given in reference 14. The computer predictions were only made for the stagnation region of the models. The results from the computer predictions for a particular test model are given in tables I, II, and IV. Computer predictions were not made for the models with parallel-fiber orientations because of the formation of the crevices. For the model design used to measure back-surface temperature rise (see fig. 7), the parallel-fiber specimens split during testing. Neither the change in nose shape of the model nor material expansion was taken into account in the computer predictions.

The thermal properties used for the computer predictions as presented in this report are given in table VI. A discussion of the sources of the properties is given in the appendix. Other combinations of thermal properties were studied; however, the present properties were better or as good as any of the various combinations.

In the computer predictions, the computations were continued until cooldown and the aerodynamic inputs were removed after the models were retracted from the stream. Effects of quenching the models with argon for the tests in the ceramic-heated tunnel were not taken into account in the computer predictions. The computer results showed that significant thermal degradation of the virgin material could occur after model retraction from the stream during the cooldown period. This continued degradation was up to 0.10 inch (0.25 cm) for the model design of figure 3 and the virgin material was always completely degraded for the model design of figure 7. The differences between the stagnation-point char thicknesses at the end of model exposure time and the end of the cooldown period are shown in figure 21.

Some typical comparisons between the experimental results and the computer predictions are shown in figures 22, 23, and 24 for the stagnation point. Although some of the results show good comparison, there is no consistency in the comparisons. In figure 25 the stagnation-point length changes of the models from the experimental and computer results are plotted as functions of total cold-wall, oxygen mass flux. As shown in figure 25(a), the length changes from the computer predictions can be adequately described with a linear least-square curve over the range of total oxygen flux. The experimental and calculated results show the same gross trend (that is Δl increasing with M_O) but the computer results overpredicted model recession at low values of M_O (where many models showed a length increase due to swelling) and, in several instances, significantly underpredicted recession when mechanical char failure occurred. The comparisons of stagnation-point char thicknesses between the experimental data and the computer predictions are shown in figure 26. The experimental char thicknesses were always greater than the computer predictions for end of model exposure time (fig. 26(a)) but had a better comparison for end of the cooldown period (fig. 26(b)). In figure 27 is shown the

comparison between the experimental data and the computer predictions for the model stagnation-point surface temperature. There is a fair agreement, the experimental temperatures being slightly higher.

Some of the experimental results could be adequately described by the ablation computer program. However, over the range of experimental results, the computer program could not adequately describe the behavior of the material. This lack of agreement is attributed to the behavior of the material during mechanical char removal, material expansion, and continued degradation during cooldown which could not be accounted for in the present analysis. Because some tests were adequately predicted by the ablation program but not the entire test series, the present study has indicated that computer predictions illustrating material behavior and defining thermal properties which are based on comparisons with a few experimental tests should be viewed with caution.

CONCLUDING REMARKS

An experimental ground-test study was conducted to evaluate the ablative characteristics of a carbon-phenolic heat-shield material designated Narmco 4028. The experimental results were compared with predictions from an ablation computer program. In addition to the study of the general ablative behavior of the material, tests were also conducted, in support of project RAM, to evaluate the effects of hole patterns in the material and the effects of injecting water through holes in the material into the flow field.

In the present tests, mechanical char removal did occur at certain test conditions depending on the mass fraction of oxygen in the stream and the stagnation pressure. For tests in nitrogen at model stagnation pressures up to 11 atmospheres (limit of the tests), the mechanical char removal did not occur. The mechanical char removal did occur for tests in air at pressures above 2.4 atmospheres and air-nitrogen mixtures above 6 atmospheres. This mechanical char removal occurred at the surface of the char and did not remove the entire char layer.

The study showed that expansion of the material occurs during testing which tends to offset the recession due to chemical removal. There is an effect of fiber orientation on the material's behavior. The models with parallel-fiber orientation formed crevices during testing and had greater recession than the models with perpendicular-fiber orientation.

The experimental data showed that holes can survive without enlargement and maintain their integrity in the material. Water injection had no significant effects on the behavior of the material in these specific tests and the holes remained free of any restrictions to the water flow.

The computer program used in the present study was successful in predicting gross trends in material behavior and for several isolated tests it gave good predictions for detailed material response. Over the broad range of experimental conditions, however, comparisons between experimental and computer results showed considerable scatter. This scatter is attributed to phenomena, such as mechanical char removal, material expansion, and material degradation during cooldown, which was not accounted for in the computer program.

Langley Research Center,
National Aeronautics and Space Administration,
Hampton, Va., July 6, 1970.

APPENDIX

SOURCES OF THE THERMAL PROPERTIES USED IN THE COMPUTER PREDICTIONS

The specific heats for the virgin material and the char were taken from reference 8. The thermal conductivities of the virgin material and the char depends upon the direction of the heat flow with respect to fiber orientation as shown by the data of reference 8. The selected thermal conductivities are based on the data of reference 8 for heat flow perpendicular to the fiber length (across fiber) which corresponds to the direction of heat flow at the model's stagnation region for perpendicular-fiber and shingled-fiber orientation of the present study. The thermal conductivity of the virgin material is taken directly from reference 8 and the thermal conductivity for the char is one-half the values given in reference 8.

The density of the virgin material was measured in the present study. There is a disagreement between measurements of the char density from reference 8 and the present study. Reference 8 gives measured char densities of 64 lbm/ft^3 (1025 kg/m^3) for char formed in a furnace and 74 lbm/ft^3 (1185 kg/m^3) for chars formed in a plasma jet. In the present study, a density of 74 lbm/ft^3 (1185 kg/m^3) was measured for chars formed in a furnace and densities from 57 to 68 lbm/ft^3 (913 to 1089 kg/m^3) for chars from several test models. Therefore, a density of 62 lbm/ft^3 (993 kg/m^3) was selected for the present study.

The heat of pyrolysis was determined from measured differential thermal analysis data. The rate constants for the thermal degradation of the virgin material was determined from measured thermal gravimetric analysis data.

The emissivity of the char was taken from the data of reference 8. The heat of combustion of the char was selected as a 10 to 20 percent increase over the value of the heat of formation of carbon monoxide being formed from graphite and oxygen. The value of the heat of sublimation of the char was selected as an average value for the sublimation of graphite. The char surface kinetics were taken from reference 15 for the "slow" kinetics of graphite.

The specific heats of the pyrolysis gas were determined from chemical equilibrium calculations based upon the elemental analysis of Narmco 4028 and the char density. This type of calculation does not account for carbon deposition. The specific heats used in the computer predictions are average values for the pressure range of the experimental program.

REFERENCES

1. Huber, Paul W.; and Sims, Theo E.: The Entry Communications Problem. Astronaut. Aeronaut., vol. 2, no. 10, Oct. 1964, pp. 30-40.
2. Sims, Theo E.: Reentry Communications Research at Langley Research Center. 1965 IEEE International Conv. Record, vol. 13, pt. 4, 1965, pp. 99-104.
3. Akey, Norman D.; and Cross, Aubrey E.: Radio Blackout Alleviation and Plasma Diagnostic Results From a 25 000 Foot Per Second Blunt-Body Reentry. NASA TN D-5615, 1970.
4. Sutton, Kenneth; Zoby, Ernest V.; and Butler, David H.: An Evaluation Test of a Full-Scale Replica of the RAM-CA Flight Heat Shield in a Rocket-Engine Exhaust. NASA TM X-1841, 1969.
5. Mechtly, E. A.: The International System of Units – Physical Constants and Conversion Factors. NASA SP-7012, 1964.
6. Sutton, Kenneth: Description and Operating Parameters of a Mach 2 Nozzle System for the Langley 11-Inch Ceramic-Heated Tunnel. NASA TN D-4750, 1968.
7. Midden, Raymond E.; and Cocke, Bennie W., Jr.: Description and Initial Calibration of the Langley 20-Inch Hypersonic Arc-Heated Tunnel. NASA TN D-4653, 1968.
8. Engelke, W. T.; Pyron, C. M., Jr.; and Pears, C. D.: Thermal and Mechanical Properties of a Nondegraded and Thermally Degraded Phenolic-Carbon Composite. NASA CR-896, 1967.
9. Starks, D. F.: Ablative Plastic Chars Containing Carbon and Graphite Reinforcements. AFML-TR-64-337, U.S. Air Force, Apr. 1965.
10. McLain, Allen G.; Sutton, Kenneth; and Walberg, Gerald D.: Experimental and Theoretical Investigation of the Ablative Performance of Five Phenolic-Nylon-Based Materials. NASA TN D-4374, 1968.
11. Exton, Reginald J.: Theory and Operation of a Variable Exposure Photographic Pyrometer Over the Temperature Range 1800° to 3600°F (1255° to 2255° K). NASA TN D-2660, 1965.
12. Fay, J.A.; and Riddell, F. R.: Theory of Stagnation Point Heat Transfer in Dissociated Air. J. Aeronaut. Sci., vol. 25, no. 2, Feb. 1958, pp. 73-85, 121.
13. Bush, Harold G.; and Dow, Marvin B.: Multidimensional Gas Flow Through Permeable Char Layers and Its Effects on Ablation. NASA TR R-296, 1969.

14. Wells, P. B.: A Method for Predicting the Thermal Response of Charring Ablation Materials. Doc. No. D2-23256, Boeing Co., 1964.

15. Scala, Sinclaire M.: The Ablation of Graphite in Dissociated Air. Part I: Theory. R62SD72, Missile and Space Div., Gen. Elec., Co., Sept. 1962.

TABLE I.- TEST CONDITIONS AND RESULTS FOR THE MODELS USED IN THE STUDY OF THE GENERAL BEHAVIOR OF THE MATERIAL

[Model design shown in fig. 3; primed values are computer values]

P_s, atm	K_o	H_s		$\dot{q}_s$		Nose shape	Fiber orientation	t, sec	Δl		x_c		T_s		Mechanical char removal	Computer prediction	$\Delta l'$		x_c' (a)		x_c' (b)		T_s'	
		Btu/lbm	MJ/kg	Btu/ft^2-sec	MW/m^2				in.	cm	in.	cm	°R	°K			in.	cm	in.	cm	in.	cm	°R	°K
0.07	0.23	11 000	25.52	680	7.72	Hemisphere	Perpendicular	30.0	+0.034	+0.086	0.28	0.71	5560	3090	No	Yes	-0.052	-0.132	0.254	0.645	0.335	0.850	5560	3090
.31	.23	10 800	25.05	1250	14.19	Hemisphere	Perpendicular	30.0	-.062	-.157	.28	.71	6060	3370	No	Yes	-.131	-.332	.227	.576	.322	.818	6060	3370
.43	.23	1 550	3.59	130	1.48	Hemisphere	Perpendicular	30.0	-.006	-.015	.24	.61	3360	1870	No	Yes	-.066	-.167	.161	.409	.200	.508	3580	1990
.60	.23	11 000	25.52	1600	18.16	Hemisphere	Perpendicular	30.0	-.114	-.290	---	---	6660	3700	No	Yes	-.184	-.467	.206	.523	.332	.843	6220	3455
.60	.23	11 000	25.52	1600	18.16	Hemisphere	Perpendicular	10.0	+.018	+.046	---	---	6760	3760	No	Yes	-.050	-.127	.152	.386	.235	.596	6170	3430
.60	.23	11 000	25.52	1600	18.16	Hemisphere	Perpendicular	20.0	-.035	-.089	---	---	6760	3760	No	Yes	-.115	-.292	.182	.462	.298	.758	6220	3455
.60	.23	11 000	25.52	1600	18.16	Hemisphere	Perpendicular	30.0	-.112	-.284	---	---	6760	3760	No	Yes	-.184	-.467	.206	.524	.332	.844	6220	3455
1.08	.08	5 500	12.76	1090	12.37	Hemisphere	Perpendicular	20.0	+.016	+.041	---	---	----	----	No	Yes	-.051	-.129	.224	.569	.295	.749	5950	3305
1.08	.08	5 000	11.60	680	7.72	Blunt	Perpendicular	20.0	-.031	-.079	---	---	5460	3035	No	Yes	-.028	-.068	.218	.554	.290	.736	5460	3035
1.38	.23	1 500	3.48	328	3.72	Hemisphere	Perpendicular	30.0	-.031	-.079	.26	.66	----	----	No	Yes	-.200	-.508	.124	.315	.171	.434	4310	2395
2.40	.23	2 340	5.43	700	7.95	Hemisphere	Perpendicular	29.3	-.448	-1.138	---	---	4460	2480	Yes	Yes	-.261	-.662	.133	.338	.190	.483	5170	2870
2.50	.08	1 900	4.41	398	4.52	Blunt	Perpendicular	20.0	+.025	+.063	---	---	4560	2540	No	Yes	-.045	-.114	.174	.442	.224	.569	4330	2450
2.50	.08	1 900	4.41	570	6.47	Hemisphere	Perpendicular	20.0	+.037	+.094	---	---	4660	2595	No	Yes	-.066	-.167	.171	.434	.221	.561	4640	2580
2.91	.23	1 500	3.48	495	5.62	Hemisphere	Perpendicular	30.0	-.159	-.404	.20	.51	----	----	Yes	Yes	-.308	-.782	.103	.262	.142	.361	4610	2560
5.88	.13	1 100	2.55	302	3.43	Blunt	Perpendicular	20.3	-.053	-.135	.18	.46	4430	2460	Yes	Yes	-.102	-.259	.117	.297	.155	.394	3750	2085
5.97	.23	1 100	2.55	304	3.45	Blunt	Perpendicular	20.0	-.137	-.348	.20	.51	4780	2655	Yes	Yes	-.175	-.444	.109	.277	.127	.323	4060	2255
5.97	.02	1 100	2.55	304	3.45	Blunt	Perpendicular	20.5	+.010	+.025	.17	.43	3760	2090	Yes	Yes	-.017	-.043	.157	.399	.188	.477	3310	1840
5.97	.02	1 100	2.55	304	3.45	Blunt	Perpendicular	29.7	+.007	+.018	.24	.61	3760	2090	Yes	Yes	-.022	-.056	.187	.475	.228	.579	3370	1870
5.97	0	1 100	2.55	304	3.45	Blunt	Perpendicular	29.9	+.022	+.056	.23	.58	3510	1950	No	Yes	.000	.000	.202	.514	.244	.620	3210	1780
6.05	.08	1 100	2.55	450	5.11	Hemisphere	Perpendicular	15.0	+.022	+.056	.14	.35	4060	2255	Yes	Yes	-.075	-.190	.110	.280	.149	.378	3780	2100
6.05	.08	1 100	2.55	450	5.11	Hemisphere	Parallel	15.0	-.040	-.102	.30	.76	4080	2270	Yes	No	-----	-----	----	----	----	----	----	----
6.05	.08	1 100	2.55	450	5.11	Hemisphere	Perpendicular	10.0	+.017	+.043	---	---	----	----	Yes	Yes	-.049	-.124	.102	.259	.132	.336	3720	2065
6.05	.08	1 100	2.55	450	5.11	Hemisphere	Perpendicular	15.0	-.014	-.035	---	---	3960	2200	Yes	Yes	-.074	-.188	.109	.277	.149	.378	3780	2100
6.05	.08	1 100	2.55	450	5.11	Hemisphere	Perpendicular	20.0	+.010	+.025	---	---	4180	2323	Yes	Yes	-.099	-.251	.126	.320	.166	.422	3780	2100
6.13	.02	1 100	2.55	456	5.18	Hemisphere	Perpendicular	30.0	+.050	+.127	---	---	3860	2145	Yes	Yes	-.039	-.099	.185	.470	.226	.574	3560	1980

[a]Char thickness at end of model exposure time.

[b]Char thickness at end of cooldown period.

TABLE I.- TEST CONDITIONS AND RESULTS FOR THE MODELS USED IN THE STUDY OF THE GENERAL BEHAVIOR OF THE MATERIAL – Concluded

P_s, atm	K_o	H_s		$\dot{q}_s$		Nose shape	Fiber orientation	t, sec	Δl		x_c		T_s		Mechanical char removal	Computer prediction	$\Delta l'$		x_c' (a)		x_c' (b)		T_s'	
		Btu/lbm	MJ/kg	Btu/ft^2-sec	MW/m^2				in.	cm	in.	cm	°R	°K			in.	cm	in.	cm	in	cm	°R	°K
6.13	0.02	1100	2.55	456	5.18	Hemisphere	Parallel	30.0	-0.068	-0.173	---	---	4110	2285	Yes	No	-----	-----	----	----	----	----	----	----
6.24	.12	1100	2.55	465	5.28	Hemisphere	Perpendicular	15.2	-.009	-.023	0.22	0.56	4300	2390	Yes	Yes	-0.112	-0.284	0.096	0.244	0.135	0.343	3950	2190
6.34	.23	1100	2.55	314	3.56	Blunt	Perpendicular	20.1	-.171	-.434	.24	.61	----	----	Yes	Yes	-.181	-.460	.090	.229	.126	.320	4090	2270
7.90	0	1100	2.55	348	3.95	Blunt	Perpendicular	25.2	+.041	-.104	.19	.48	3330	1850	No	No	-----	-----	----	----	----	----	----	----
8.62	.08	1100	2.55	540	6.13	Hemisphere	Perpendicular	15.2	-.036	-.091	.18	.46	4180	2320	Yes	Yes	-.088	-.224	.108	.274	.147	.374	3860	2140
8.62	.08	1100	2.55	540	6.13	Hemisphere	Parallel	15.1	-.097	-.246	.25	.63	4180	2320	Yes	No	-----	-----	----	----	----	----	----	----
10.00	0	1100	2.55	392	4.45	Blunt	Perpendicular	39.4	+.018	+.046	---	---	3720	2070	No	Yes	-.000	-.000	.234	.595	.287	.729	3880	2155
10.41	.13	1100	2.55	400	4.54	Blunt	Perpendicular	20.1	-.241	-.612	.18	.46	4160	2310	Yes	Yes	-.137	-.348	.104	.264	.141	.358	3930	2180
10.60	0	1100	2.55	404	4.59	Blunt	Perpendicular	20.2	+.018	+.046	.21	.53	3580	1990	No	Yes	.000	.000	.170	.432	.222	.564	3350	1860
10.72	.23	1100	2.55	592	6.72	Hemisphere	Perpendicular	20.2	-.518	-1.316	.16	.41	4730	2630	Yes	Yes	-.348	-.885	.075	.190	.083	----	4380	2430
10.78	.13	1100	2.55	397	4.51	Blunt	Parallel	20.0	-.361	-.920	.12	.30	4550	2530	Yes	No	-----	-----	----	----	----	----	----	----
10.78	.02	1100	2.55	606	6.88	Hemisphere	Perpendicular	30.7	-.018	-.046	---	---	3780	2100	Yes	Yes	-.054	-.137	.183	.465	.234	.595	3670	2040
10.78	0	1100	2.55	606	6.88	Hemisphere	Perpendicular	30.7	+.067	+.170	---	---	3780	2100	No	Yes	.000	.000	.223	.566	.254	.645	3560	1980
10.78	0	1100	2.55	606	6.88	Hemisphere	Parallel	30.4	+.009	+.023	---	---	3810	2115	No	No	-----	-----	----	----	----	----	----	----
10.91	.09	822	1.91	426	4.84	Hemisphere	Perpendicular	15.7	-.190	-.483	.13	.33	3840	2135	Yes	Yes	-.113	-.287	.087	.221	.115	.292	3380	1880
10.91	.09	822	1.91	426	4.84	Hemisphere	Parallel	15.2	-.220	-.559	.12	.30	3760	2090	Yes	No	-----	-----	----	----	----	----	----	----
10.93	.02	1100	2.55	411	4.66	Blunt	Perpendicular	20.4	+.012	+.030	.21	.53	3960	2200	Yes	Yes	-.024	-.061	.156	.396	.198	.503	3950	2195
11.00	.10	1100	2.55	610	6.92	Hemisphere	Perpendicular	10.0	-.083	-.211	---	---	3810	2115	Yes	Yes	-.083	-.211	.079	.200	.119	.302	3950	2195
11.00	.10	1100	2.55	610	6.92	Hemisphere	Perpendicular	15.0	-.129	-.328	---	---	4360	2420	Yes	Yes	-.125	-.318	.086	.218	.124	.315	4000	2220
11.00	.10	1100	2.55	610	6.92	Hemisphere	Perpendicular	20.0	-.239	-.606	---	---	4160	2310	Yes	Yes	-.168	-.427	.091	.231	.128	.325	4050	2250
11.26	.09	1100	2.55	620	7.04	Hemisphere	Perpendicular	15.0	-.114	-.290	.18	.46	4290	2380	Yes	Yes	-.117	-.297	.096	.244	.134	.340	3950	2190
11.26	.09	1100	2.55	620	7.04	Hemisphere	Parallel	15.0	-.225	-.571	.18	.46	4310	2395	Yes	No	-----	-----	----	----	----	----	----	----

[a]Char thickness at end of model exposure time.

[b]Char thickness at end of cooldown period.

TABLE II.- TEST CONDITIONS AND RESULTS FOR THE MODELS USED TO STUDY THE EFFECTS OF FIBER ORIENTATION

[Model design shown in fig. 4]

p_s, atm	K_o	H_s		$\dot{q}_s$		Fiber orientation	t, sec	Δl		x_c		T_s		Mechanical char removal	Computer prediction	$\Delta l'$		x_c' (a)		x_c' (b)		T_s'	
		Btu/lbm	MJ/kg	Btu/ft^2-sec	MW/m^2			in.	cm	in.	cm	^oR	^oK			in.	cm	in.	cm	in.	cm	^oR	^oK
0.60	0.23	11 000	25.52	1600	18.16	Parallel	9.3	-0.040	-0.102	0.26	0.66	----	----	No	No	-----	-----	----	----	----	----	----	----
.60	.23	11 000	25.52	1600	18.16	Perpendicular	4.5	+.032	+.081	.20	.51	5960	3310	No	Yes	-0.018	-0.046	0.102	0.359	0.152	0.386	6000	3330
.60	.23	11 000	25.52	1600	18.16	Shingled	3.6	-.006	-.015	.16	.41	5860	3260	No	Yes	-.013	-.033	.089	.226	.137	.348	5860	3260
2.50	.12	1 950	4.53	600	6.81	Parallel	12.5	-.052	-.132	---	---	4860	2700	No	No	-----	-----	----	----	----	----	----	----
2.50	.12	1 950	4.53	600	6.81	Perpendicular	16.2	-.039	-.086	---	---	4860	2700	No	Yes	-.082	-.204	.127	.322	.192	.487	4740	2630
2.50	.12	1 950	4.53	600	6.81	Shingled	14.3	-.042	-.107	---	---	4660	2590	No	Yes	-.071	-.180	.121	.308	.181	.460	4710	2620
6.05	.08	1 100	2.55	450	5.11	Parallel	14.3	-----	-----	---	---	----	----	Yes	No	-----	-----	----	----	----	----	----	----
6.05	.08	1 100	2.55	450	5.11	Perpendicular	16.5	-.036	-.091	.25	.63	4000	2220	Yes	Yes	-.080	-.203	.104	.264	.145	.368	3750	2080
6.05	.08	1 100	2.55	450	5.11	Shingled	15.4	-.042	-.107	.22	.56	----	----	Yes	Yes	-.074	-.188	.098	.249	.135	.343	3750	2080
11.00	.10	1 100	2.55	610	6.93	Parallel	12.5	-----	-----	---	---	4360	2420	Yes	No	-----	-----	----	----	----	----	----	----
11.00	.10	1 100	2.55	610	6.93	Perpendicular	14.2	-----	-----	---	---	4580	2545	Yes	Yes	-.116	-.295	.079	.201	.114	.290	4000	2220
11.00	.10	1 100	2.55	610	6.93	Shingled	15.2	-.185	-.470	---	---	4260	2370	Yes	Yes	-.125	-.318	.082	.208	.122	.310	4000	2220

[a]Char thickness at end of model exposure time.

[b]Char thickness at end of cooldown period.

TABLE III.- TEST CONDITIONS AND RESULTS FOR THE MODELS USED TO STUDY THE EFFECTS OF WATER INJECTION

[Model design shown in fig. 6]

p_s, atm	K_o	H_s		$\dot{q}_s$		Injection position	t, sec	Δl		x_c		T_s		Mechanical char removal	$\dot{w}$	
		Btu/lbm	MJ/kg	Btu/ft^2-sec	MW/m^2			in.	cm	in.	cm	°R	°K		lbm/sec	kg/s
0.60	0.23	11 000	25.52	1600	18.16	Stagnation	5.0	+0.018	+0.046	0.10	0.25	5300	2945	No	0.024	0.011
.60	.23	11 000	25.52	1600	18.16	Sidewall	5.0	+.029	+.074	.21	.53	5300	2945	No	.035	.016
11.00	.10	1 100	2.55	610	6.93	Stagnation	10.0	-.085	-.216	---	---	4060	2255	Yes	.023	.010
11.00	.10	1 100	2.55	610	6.93	Sidewall	10.0	-.130	-.330	---	---	4460	2475	Yes	.080	.036
11.00	.10	1 100	2.55	610	6.93	Stagnation	10.0	-.081	-.206	.08	.20	4060	2255	Yes	.059	.027
11.00	.10	1 100	2.55	610	6.93	Sidewall	10.0	-.140	-.356	.12	.30	4360	2425	Yes	.135	.061

TABLE IV.- TEST CONDITIONS AND RESULTS FOR THE MODELS USED IN THE MEASUREMENT OF BACKSURFACE TEMPERATURE RISE

[Model design shown in fig. 7]

p_s, atm	K_o	H_s		$\dot{q}_s$		Fiber orientation	t, sec	Δl		x_c		T_s		Note	Computer prediction	$\Delta l'$		x_c' (a)		x_c' (b)		T_s'	
		Btu/lbm	MJ/kg	Btu/ft^2-sec	MW/m^2			in.	cm	in.	cm	°R	°K			in.	cm	in.	cm	in.	cm	°R	°K
0.07	0.23	5 000	11.60	128	1.45	Perpendicular	62.2	+0.007	+0.018	0.41	1.04	3960	2200		Yes	-0.037	-0.094	0.257	0.653	0.500	1.270	3740	2080
.07	.23	11 500	26.68	285	3.24	Perpendicular	61.0	-.015	-.038	.49	1.24	4820	2680		Yes	-.035	-.089	.314	.797	.500	1.270	4680	2600
.07	.23	12 500	29.00	310	3.52	Parallel	42.0	+.002	+.005	.50	1.27	4860	2700	Split	No	-----	-----	----	----	----	----	----	----
.07	.23	10 700	24.82	270	3.06	Perpendicular	57.5	-.003	-.008	.50	1.27	5410	3005		Yes	-.032	-.081	.304	.772	.500	1.270	4570	2540
.32	.23	11 500	26.68	621	7.05	Perpendicular	35.5	-.037	-.094	.46	1.17	6060	3363		Yes	-.049	-.125	.269	.687	.500	1.270	5670	3150
.32	.23	12 100	28.07	655	7.44	Parallel	28.2	-.011	-.028	.49	1.24	5590	3105	Split	No	-----	-----	----	----	----	----	----	----

[a]Char thickness at end of model exposure time.

[b]Char thickness at end of cooldown period.

TABLE V.- ELEMENTAL ANALYSIS OF NARMCO 4028

[Percentages by weight]

Carbon	83.63
Oxygen	10.79
Hydrogen	3.44
Nitrogen	0.38
Ash	0.56
Total	98.80

TABLE VI.- THERMAL PROPERTIES USED IN COMPUTER PREDICTIONS

(a) Virgin material

Density	87 lbm/ft^3	(1392 kg/m^3)
Specific heat:	Btu/lbm-^oR	kJ/kg-K
460° R (256 K)	0.238	0.99
560° R (311 K)	0.292	1.22
660° R (367 K)	0.317	1.33
760° R (422 K)	0.332	1.39
860° R (477 K)	0.346	1.45
960° R (533 K)	0.360	1.51
1060° R (589 K)	0.374	1.56
1160° R (644 K)	0.388	1.62
1260° R (700 K)	0.402	1.68
1460° R (811 K)	0.430	1.80
Thermal conductivity:	Btu/ft-sec-^oR	W/m-K
460° R (256 K)	0.90×10^{-4}	0.561
560° R (311 K)	1.02×10^{-4}	0.636
660° R (367 K)	1.11×10^{-4}	0.693
760° R (422 K)	1.19×10^{-4}	0.742
860° R (477 K)	1.24×10^{-4}	0.774
960° R (533 K)	1.24×10^{-4}	0.774
1060° R (589 K)	1.19×10^{-4}	0.742
1160° R (644 K)	1.12×10^{-4}	0.698
1260° R (700 K)	1.01×10^{-4}	0.630
1460° R (811 K)	0.77×10^{-4}	0.479
Heat of pyrolysis	200 Btu/lbm	(0.465 MJ/kg)
Rate constants for thermal degradation:		
First frequency factor	2.9311×10^{15} lbm/ft^3-sec	(4.70×10^{16} kg/m^3-s)
First activation energy	4.88×10^4 calories/mole	(0.204 MJ/mole)
Second frequency factor	3.0975×10^{13} lbm/ft^3-sec	(4.96×10^{14} kg/m^3-s)
Second activation energy	5.01×10^4 calories/mole	(0.209 MJ/mole)

TABLE VI.- THERMAL PROPERTIES USED IN COMPUTER PREDICTIONS - Continued

(b) Charred material

Density	62 lbm/ft^3	(1184 kg/m^3)
Specific heat:	Btu/lbm-$^\circ$R	kJ/kg-K
500° R (278 K)	0.240	1.00
1000° R (556 K)	0.330	1.38
1460° R (811 K)	0.385	1.61
1960° R (1089 K)	0.445	1.86
2460° R (1366 K)	0.480	2.01
2960° R (1645 K)	0.495	2.06
3460° R (1923 K)	0.505	2.11
3960° R (2200 K)	0.515	2.15
4460° R (2478 K)	0.520	2.17
4960° R (2756 K)	0.525	2.19
5460° R (3030 K)	0.530	2.21
5960° R (3311 K)	0.535	2.24
6460° R (3590 K)	0.540	2.26
6960° R (3867 K)	0.545	2.28
Thermal conductivity:	Btu/ft-sec-$^\circ$R	W/m-K
500° R (278 K)	0.13×10^{-3}	0.810
1000° R (556 K)	0.14×10^{-3}	0.872
1460° R (811 K)	0.15×10^{-3}	0.935
1960° R (1089 K)	0.16×10^{-3}	0.977
2460° R (1366 K)	0.18×10^{-3}	1.128
2960° R (1645 K)	0.19×10^{-3}	1.189
3210° R (1782 K)	0.21×10^{-3}	1.314
3460° R (1923 K)	0.24×10^{-3}	1.502
3960° R (2200 K)	0.33×10^{-3}	2.065
4460° R (2478 K)	0.43×10^{-3}	2.790
4710° R (2617 K)	0.48×10^{-3}	3.002
4960° R (2756 K)	0.56×10^{-3}	3.502
5460° R (3030 K)	0.78×10^{-3}	4.880
5960° R (3311 K)	1.02×10^{-3}	6.390
6400° R (3555 K)	1.18×10^{-3}	7.380
6800° R (3778 K)	1.49×10^{-3}	9.325
Char surface emissivity		0.7
Char heat of combustion	5100 Btu/lbm	(11.82 MJ/kg)
Char heat of sublimation	9000 Btu/lbm	(20.88 MJ/kg)
Char surface kinetics:		
Frequency factor	4.47×10^4 lbm/ft^2-sec-atm$^{1/2}$	(21.8×10^4 kg/m^2-s-atm$^{1/2}$)
Activation energy	42.3 kcal/mole	(0.177 MJ/mole)
Reaction order		0.5

TABLE VI.- THERMAL PROPERTIES USED IN COMPUTER PREDICTIONS - Concluded

(c) Pyrolysis gas

Specific heat:	Btu/lbm-$^{\circ}$R	kJ/kg-K
500° R (278 K)	0.75	3.14
1000° R (556 K)	1.00	4.18
1460° R (817 K)	1.50	6.28
1960° R (1089 K)	2.00	8.36
2460° R (1366 K)	1.00	4.18
2960° R (1645 K)	1.00	4.18
3460° R (1923 K)	1.00	4.18
3960° R (2200 K)	1.00	4.18
4460° R (2478 K)	1.75	7.32
4960° R (2756 K)	2.50	10.47
5460° R (3030 K)	4.50	18.85
5960° R (3311 K)	7.50	31.40
6460° R (3590 K)	9.50	39.75
6960° R (3867 K)	10.00	41.84

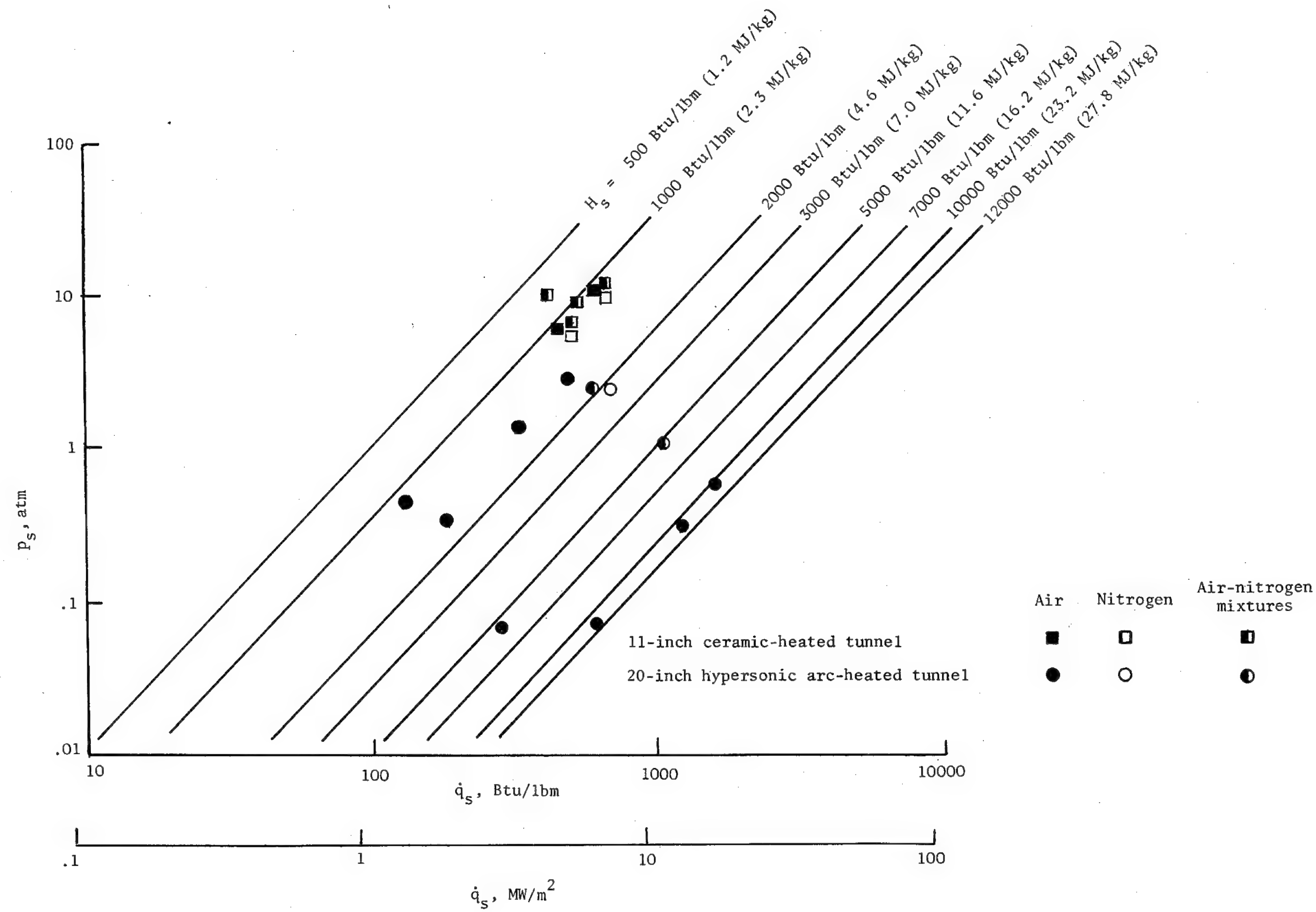

Figure 1.- Test conditions for a 1-inch-diameter (2.54 cm) hemispherical model.

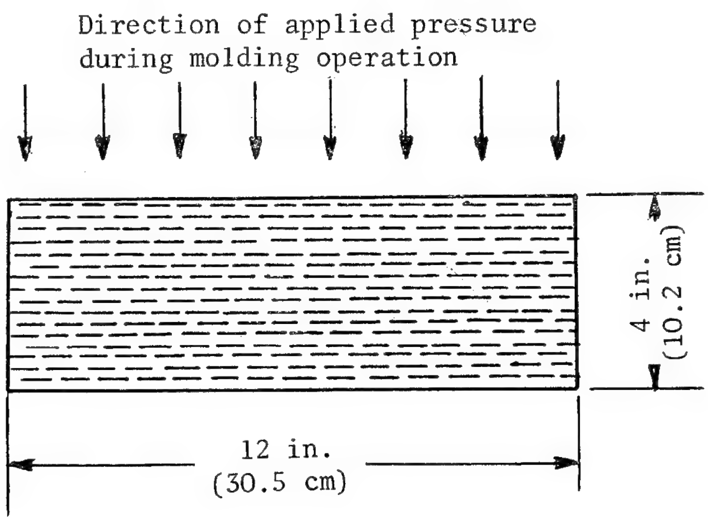

Figure 2.- Sketch of fiber orientation in molded billets.

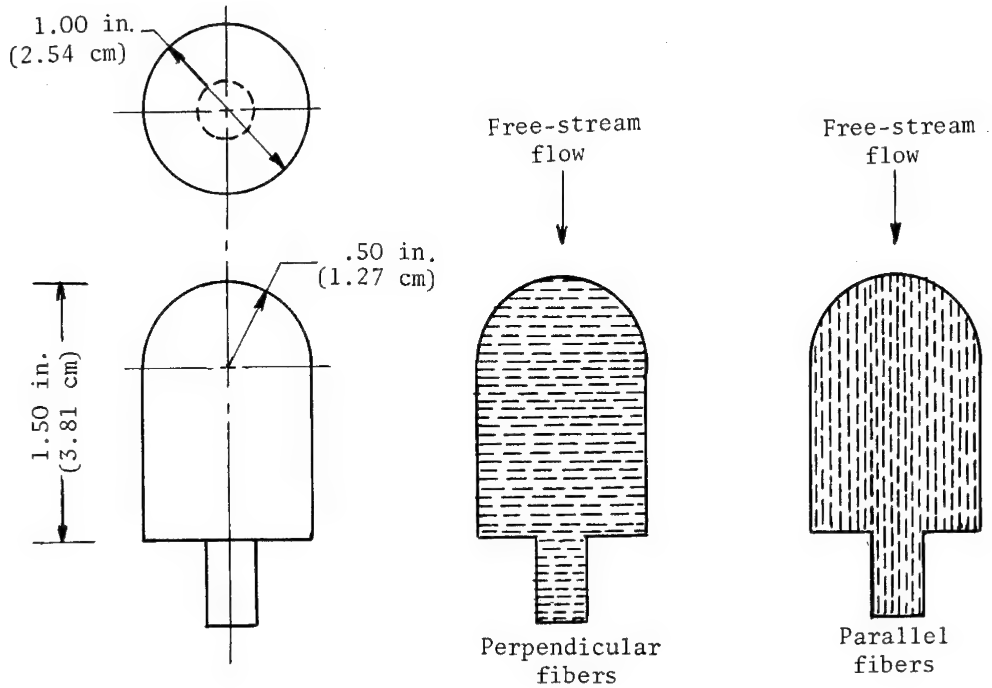

(a) Hemispherical nose.

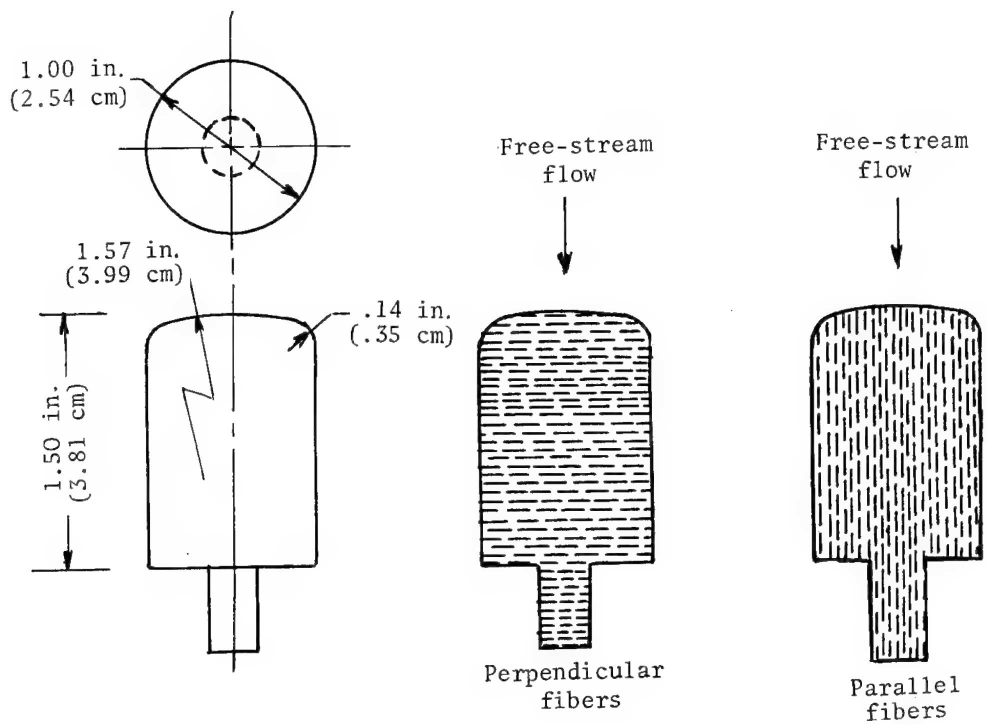

(b) Blunt nose.

Figure 3.- Model design used for the study of the general behavior of the material.

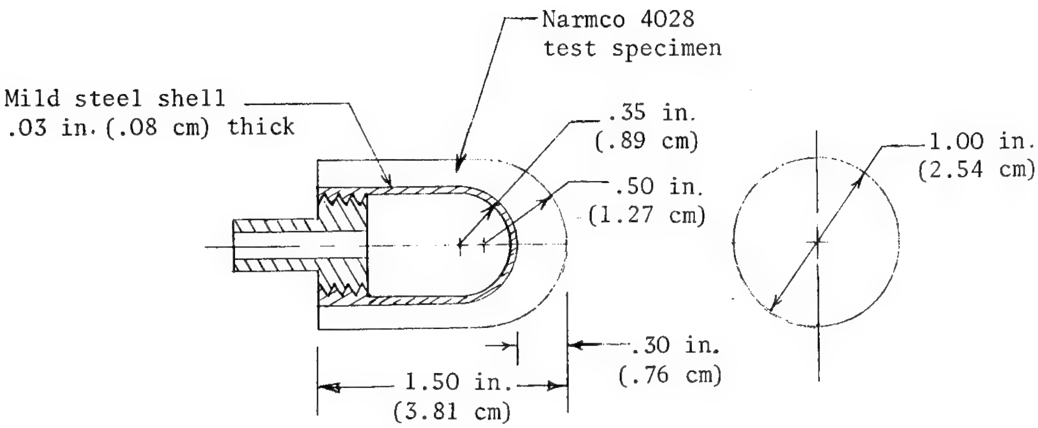

(a) Model construction.

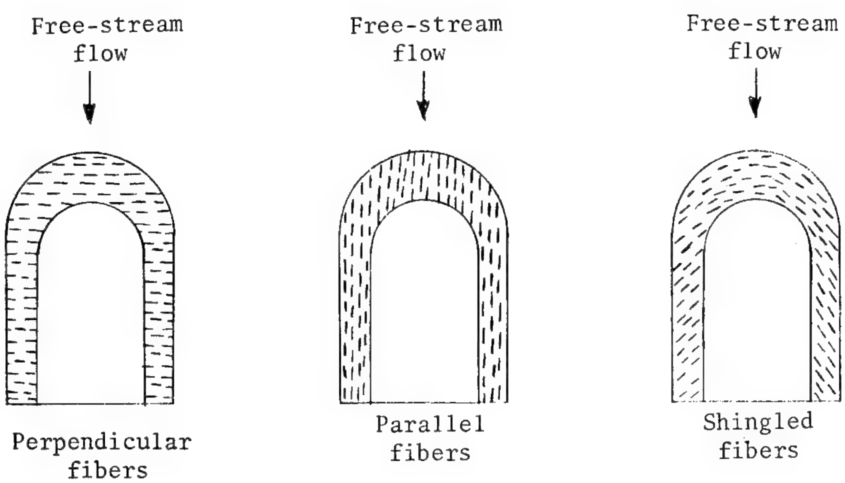

(b) Fiber orientation in test specimen.

Figure 4.- Model design used to study the effect of fiber orientation.

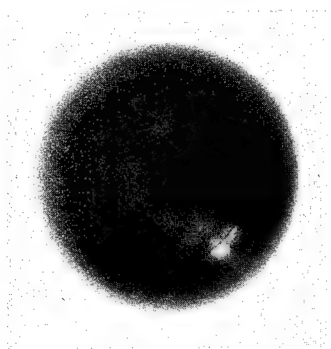

No holes

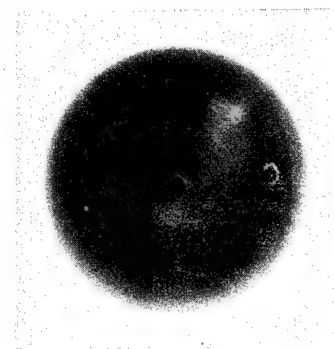

1 hole

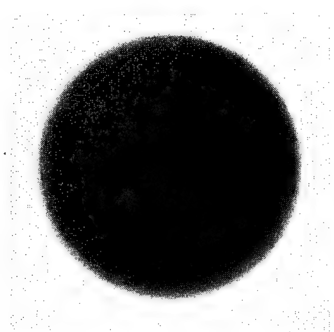

4 holes

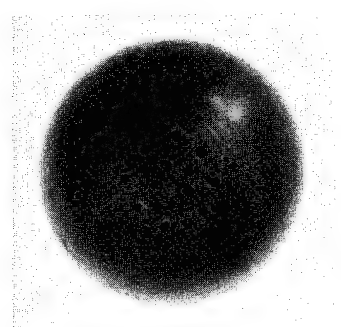

13 holes

L-70-4707

Figure 5.- Photographs of the top view of the models used in the study of the effect of holes in the material. The holes were drilled in the hemispherical models shown in figure 3(a) with perpendicular-fiber orientation.

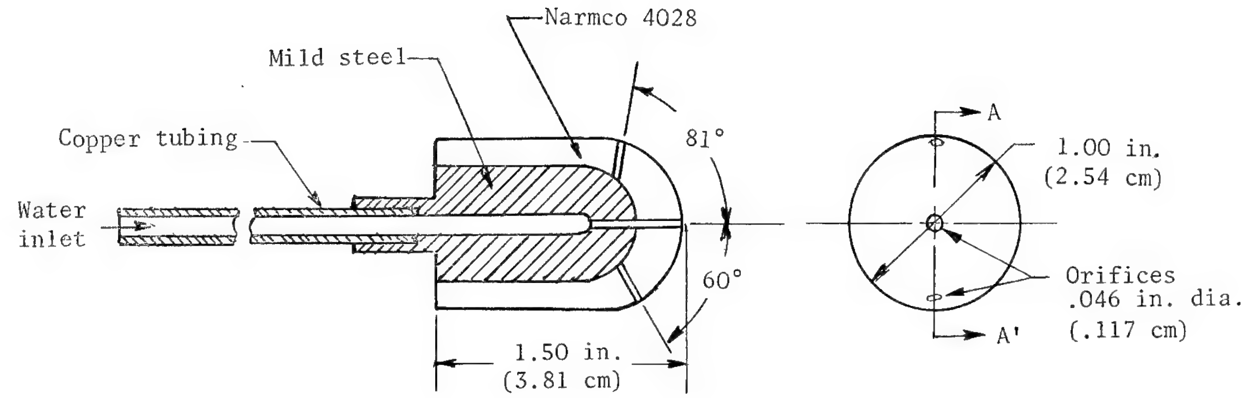

Section A-A'

(a) Stagnation-point injection.

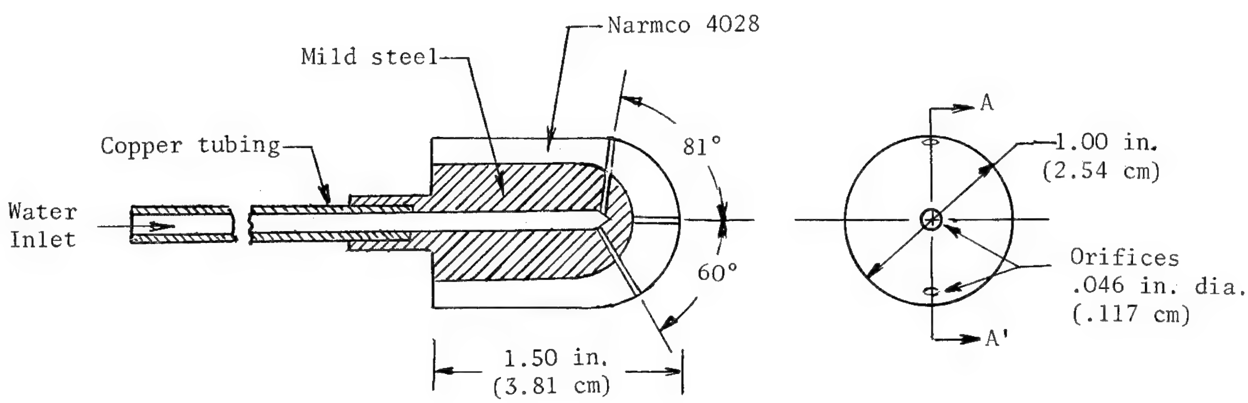

Section A-A'

(b) Side injection.

Figure 6.- Model design used to study the effect of water injection. Test specimen had shingled-fiber orientation as shown in figure 4(b).

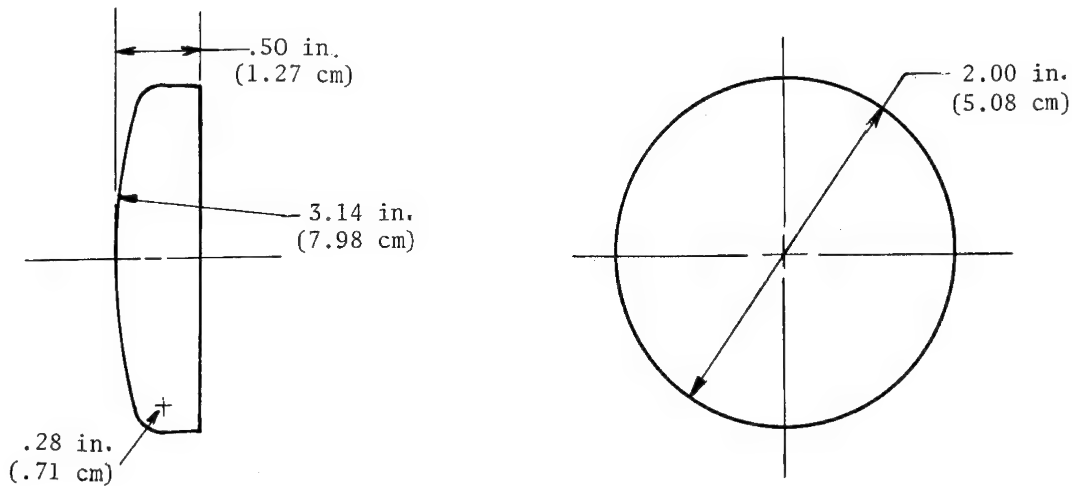

(a) Shape of material test specimen.

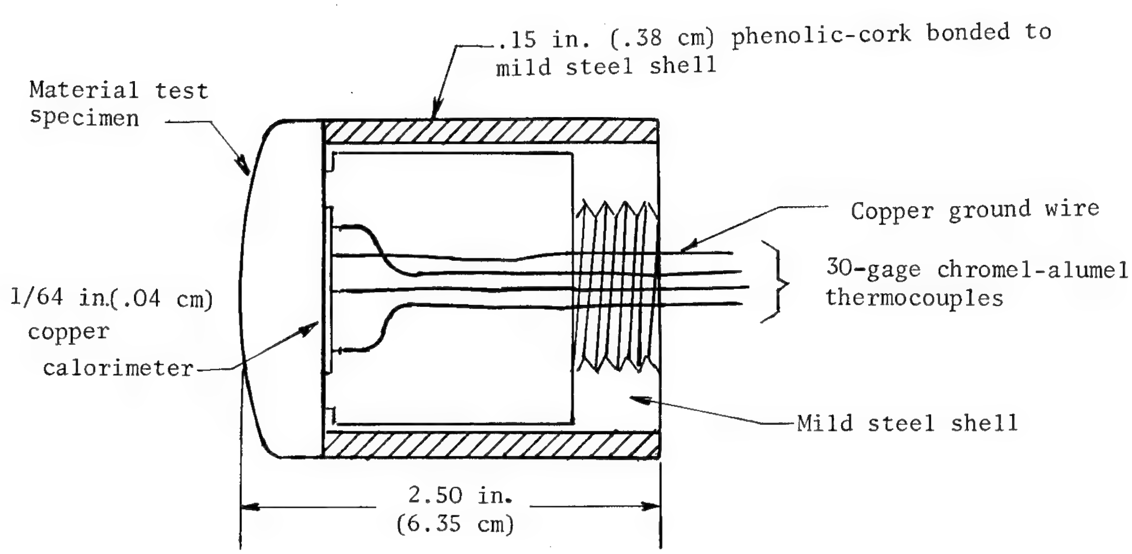

(b) Material specimen and thermocouple assembly.

Figure 7.- Model design used in the evaluation of the thermal properties.

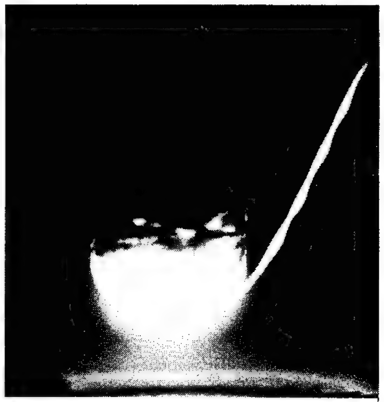

(a) Hemispherical-nose model.
$p_s = 2.40$ atm; $K_o = 0.23$.
$\dot{q}_s = 700$ Btu/ft^2-sec (7.95 MW/m^2);
$H_s = 2340$ Btu/lbm (5.43 MJ/kg).

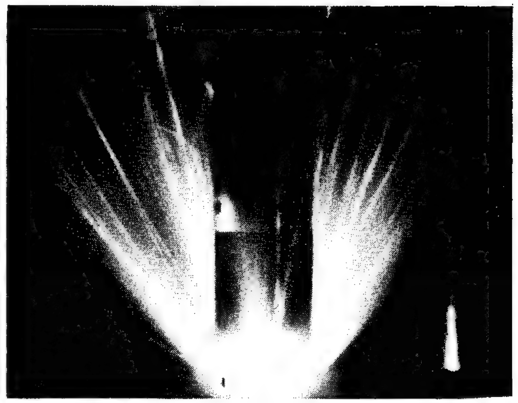

(b) Blunt-nose model.
$p_s = 10.41$ atm; $K_o = 0.13$;
$\dot{q}_s = 400$ Btu/ft^2-sec (4.54 MW/m^2);
$H_s = 1100$ Btu/lbm (2.55 MJ/kg).

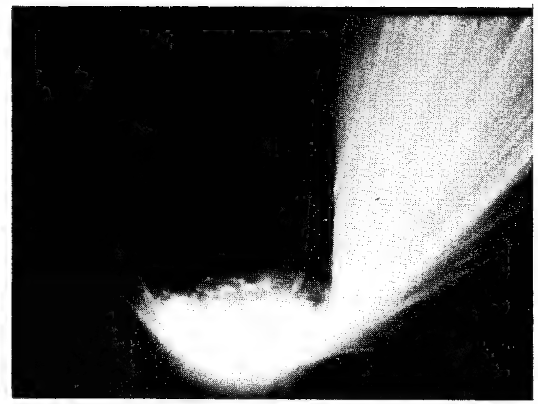

L-70-4708

(c) Hemispherical-nose model.
$p_s = 11.26$ atm; $K_o = 0.09$;
$\dot{q}_s = 620$ Btu/ft^2-sec (7.04 MW/m^2);
$H_s = 1100$ Btu/lbm (2.55 MJ/kg).

Figure 8.- Photographs showing mechanical char removal from the models during testing. Model design as shown in figure 3 with perpendicular-fiber orientation.

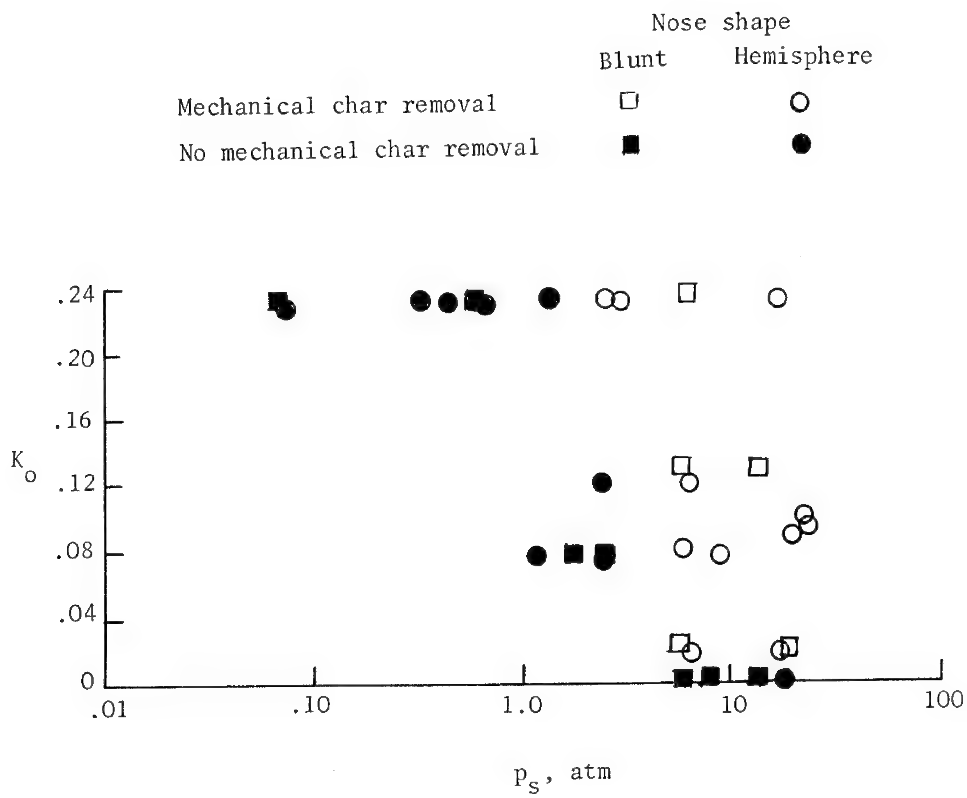

Figure 9.- Test environments at which mechanical char removal occurred. Fiber orientation in the material was perpendicular to the free-stream flow.

p_s = .07 atm.; K_o = .23
$\dot{q}_s$ = 680 Btu/ft^2-sec
(7.72 MW/m^2)
H_s = 11,000 Btu/lbm
(25.50 MJ/kg)
t = 30.0 seconds

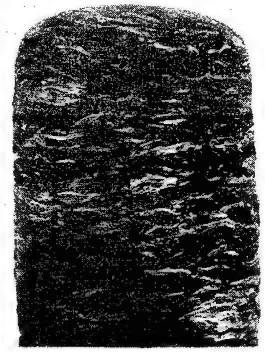

p_s = .60 atm.; K_o = .23
$\dot{q}_s$ = 1600 Btu/ft^2-sec
(18.20 MW/m^2)
H_s = 11,000 Btu/lbm
(25.50 MJ/kg)
t = 30.0 seconds

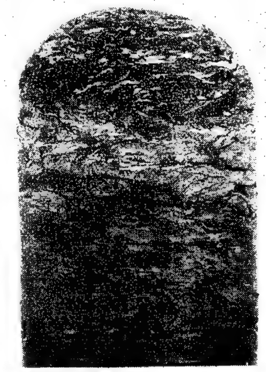

p_s = 1.38 atm.; K_o = .23
$\dot{q}_s$ = 328 Btu/ft^2-sec
(3.72 MW/m^2)
H_s = 1500 Btu/lbm
(3.48 MJ/kg)
t = 30.0 seconds

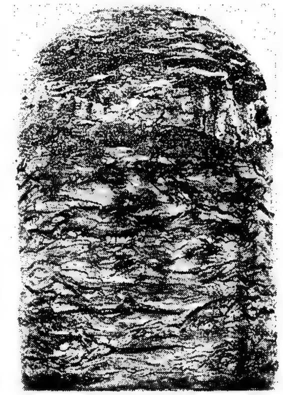

p_s = 2.50 atm.; K_o = .08
$\dot{q}_s$ = 570 Btu/ft^2-sec
(6.47 MW/m^2)
H_s = 1900 Btu/lbm
(4.41 MJ/kg)
t = 20.0 seconds

p_s = 2.91 atm.; K_o = .23
$\dot{q}_s$ = 495 Btu/ft^2-sec
(5.62 MW/m^2)
H_s = 1500 Btu/lbm
(3.48 MJ/kg)
t = 30.0 seconds

p_s = 6.05 atm.; K_o = .08
$\dot{q}_s$ = 450 Btu/ft^2-sec
(5.11 MW/m^2)
H_s = 1100 Btu/lbm
(2.55 MJ/kg)
t = 20.0 seconds

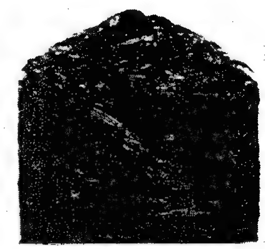

p_s = 10.72 atm.; K_o = .23
$\dot{q}_s$ = 592 Btu/ft^2-sec
(6.72 MW/m^2)
H_s = 1100 Btu/lbm
(2.55 MJ/kg)
t = 20.2 seconds

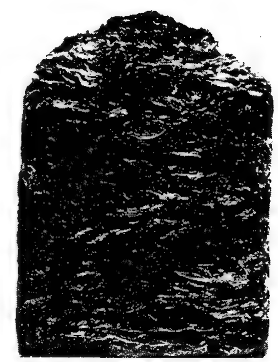

p_s = 11.26 atm.; K_o = .09
$\dot{q}_s$ = 620 Btu/ft^2-sec
(7.04 MW/m^2)
H_s = 1100 Btu/lbm
(2.55 MJ/kg)
t = 15.0 seconds

(a) Hemispherical-nose models.

L-70-4709

Figure 10.- Photographs of representative models showing the regime of mechanical char removal. Fiber orientation in the material was perpendicular to the free-stream flow.

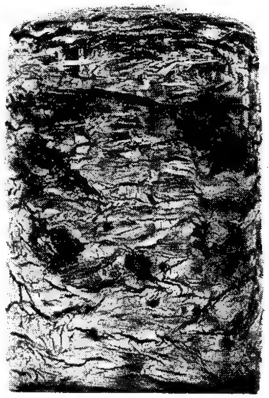

p_s = 2.50 atm.; K_o = .08
$\dot{q}_s$ = 398 Btu/ft^2-sec
(4.48 MW/m^2)
H_s = 1900 Btu/lbm
(4.41 MJ/kg)
t = 20.0 seconds

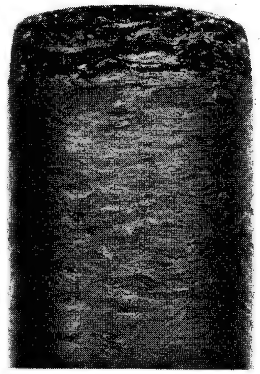

p_s = 5.97 atm.; K_o = 0
$\dot{q}_s$ = 304 Btu/ft^2-sec
(3.42 MW/m^2)
H_s = 1100 Btu/lbm
(2.55 MJ/kg)
t = 29.9 seconds

p_s = 5.97 atm.; K_o =.02
$\dot{q}_s$ = 304 Btu/ft^2-sec
(3.42 MW/m^2)
H_s = 1100 Btu/lbm
(2.55 MJ/kg)
t = 29.7 seconds

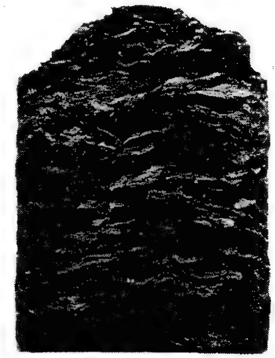

p_s = 5.88 atm.; K_o = .13
$\dot{q}_s$ = 302 Btu/ft^2-sec
(3.40 MW/m^2)
H_s = 1100 Btu/lbm
(2.55 MJ/kg)
t = 20.3 seconds

p_s = 5.97 atm.; K_o = .23
$\dot{q}_s$ = 304 Btu/ft^2-sec
(3.42 MW/m^2)
H_s = 1100 Btu/lbm
(2.55 MJ/kg)
t = 20.0 seconds

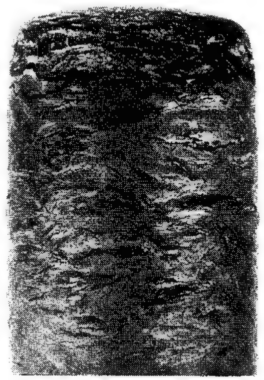

p_s = 10.60 atm.; K_o = 0
$\dot{q}_s$ = 404 Btu/ft^2-sec
(4.55 MW/m^2)
H_s = 1100 Btu/lbm
(2.55 MJ/kg)
t = 20.2 seconds

p_s = 10.93 atm.; K_o = .02
$\dot{q}_s$ = 411 Btu/ft^2-sec
(4.63 MW/m^2)
H_s = 1100 Btu/lbm
(2.55 MJ/kg)
t = 20.4 seconds

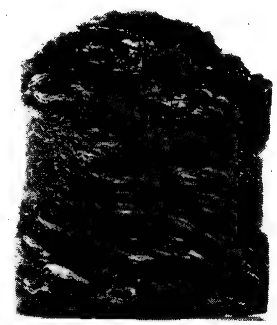

p_s = 10.41 atm.; K_o = .13
$\dot{q}_s$ = 400 Btu/ft^2-sec
(4.50 MW/m^2)
H_s = 1100 Btu/lbm
(2.55 MJ/kg)
t = 20.1 seconds

L-70-4710

(b) Blunt-nose models.

Figure 10.- Concluded.

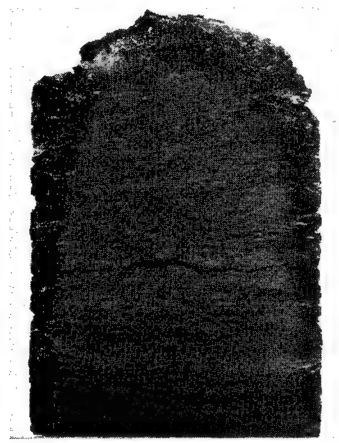

L-70-4711

(a) Hemispherical-nose model.
$p_s = 11.26$ atm; $K_o = 0.09$;
$\dot{q}_s = 620$ Btu/ft^2-sec
(7.04 MW/m^2);
$H_s = 1100$ Btu/lbm
(2.55 MJ/kg);
$t = 15.0$ seconds.

(b) Blunt-nose model.
$p_s = 5.88$ atm; $K_o = 0.13$;
$\dot{q}_s = 302$ Btu/ft^2-sec
(3.42 MW/m^2);
$H_s = 1100$ Btu/lbm
(2.55 MJ/kg);
$t = 20.3$ seconds.

Figure 11.- Photographs of sectioned models showing the char thickness for models which experienced mechanical char removal.

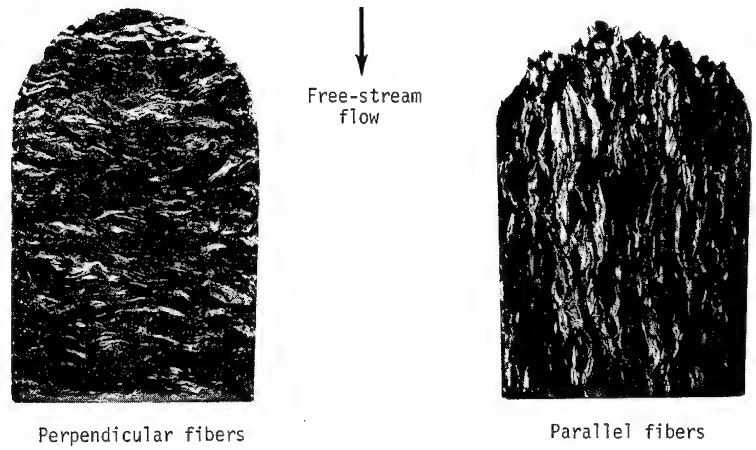

(a) $p_s = 6.05$ atm; $K_o = 0.08$;
$\dot{q}_s = 450$ Btu/ft^2-sec (5.18 MW/m^2);
$H_s = 1100$ Btu/lbm (2.55 MJ/kg);
$t = 15.0$ seconds.

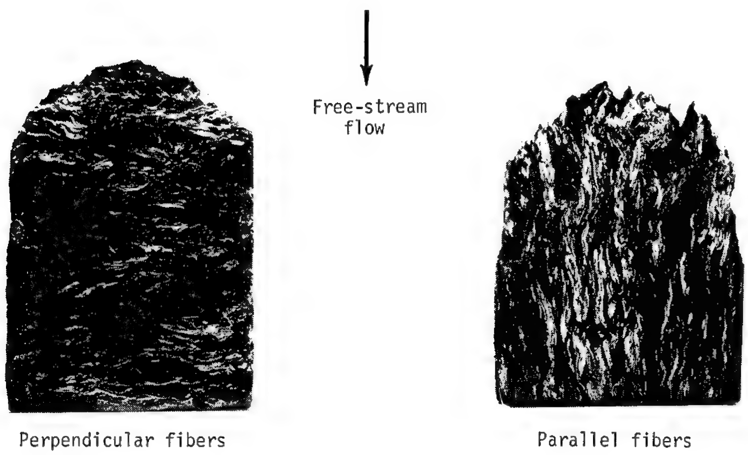

L-70-4712

(b) $p_s = 11.26$ atm; $K_o = 0.09$;
$\dot{q}_s = 620$ Btu/ft^2-sec (7.04 MW/m^2);
$H_s = 1100$ Btu/lbm (2.55 MJ/kg);
$t = 15.0$ seconds.

Figure 12.- Photographs of representative models (after testing) showing the effect of perpendicular- and parallel-fiber orientation on the behavior of the material. Models are of the hemispherical-nose design as shown in figure 3.

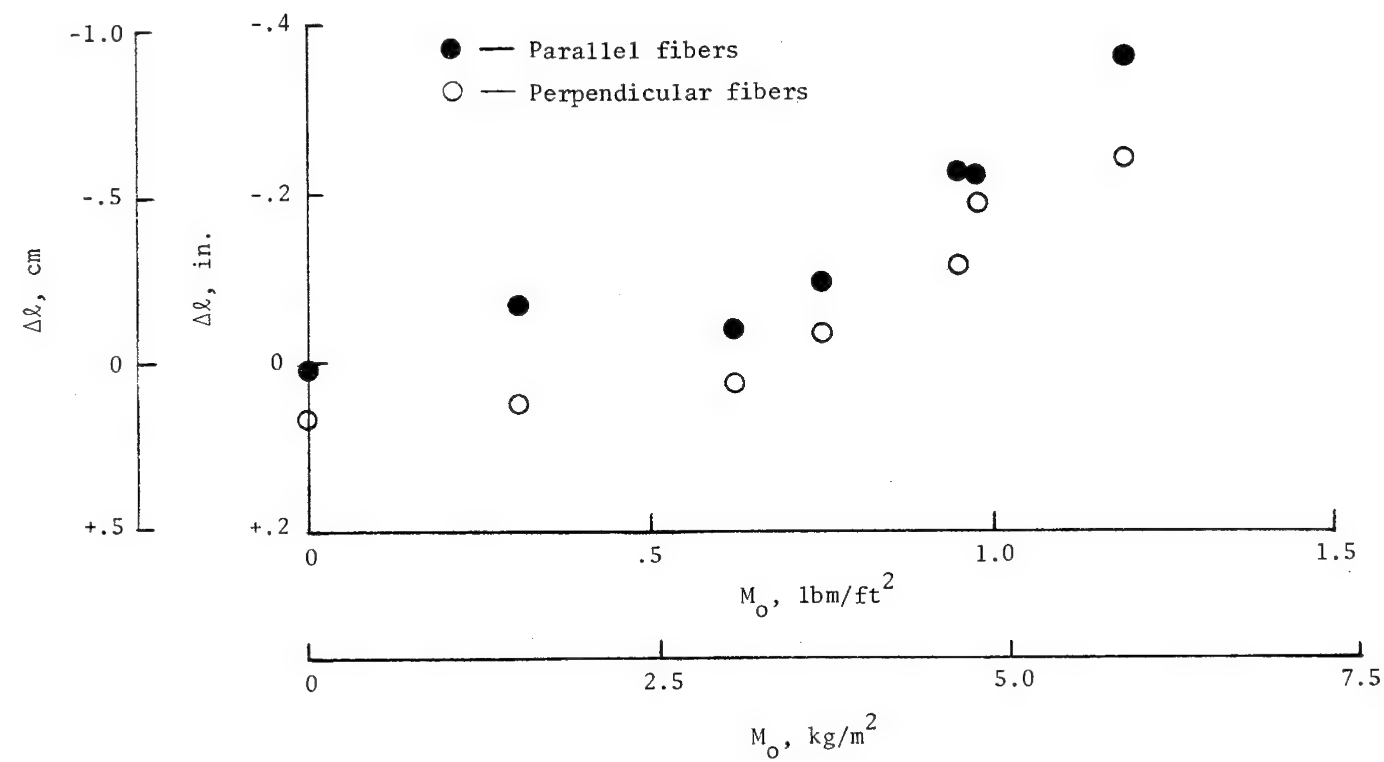

Figure 13.- The stagnation-point length change comparison for models with parallel- and perpendicular-fiber orientation tested at comparable conditions. The abscissa coordinate is the total cold-wall oxygen mass flux.

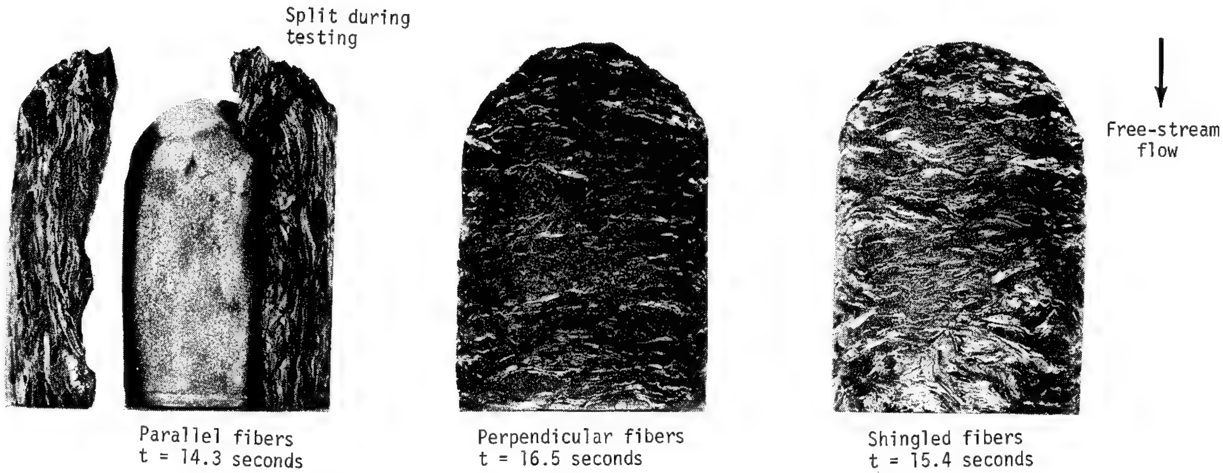

(a) $p_s = 6.05$ atm; $K_o = 0.08$; $\dot{q}_s = 450$ Btu/ft^2-sec (5.11 MW/m^2); $H_s = 1100$ Btu/lbm (2.55 MJ/kg).

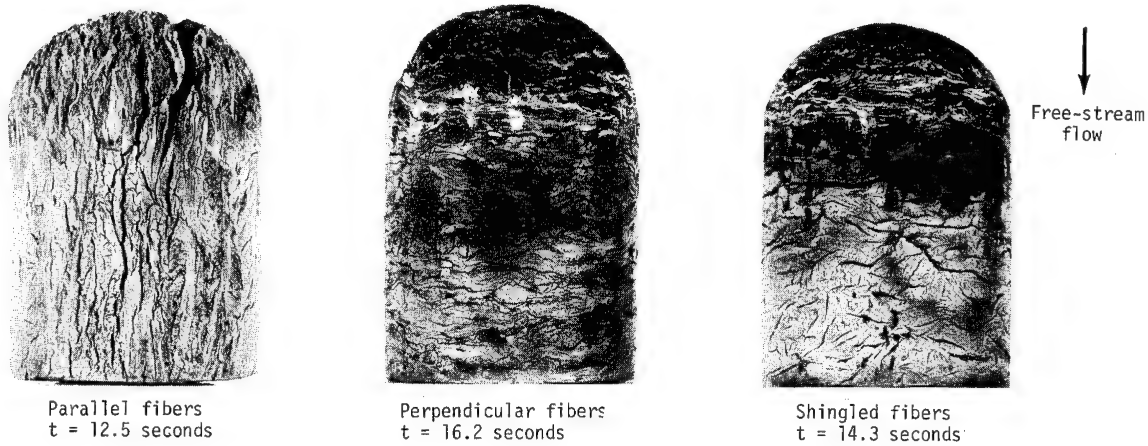

L-70-4713

(b) $p_s = 2.50$ atm; $K_o = 0.12$; $\dot{q}_s = 600$ Btu/ft^2-sec (6.81 MW/m^2); $H_s = 1950$ Btu/lbm (4.53 MJ/kg).

Figure 14.- Photographs of representative models (after testing) showing the effect of three different fiber orientations on the behavior of the material. Models are of the design shown in figure 4.

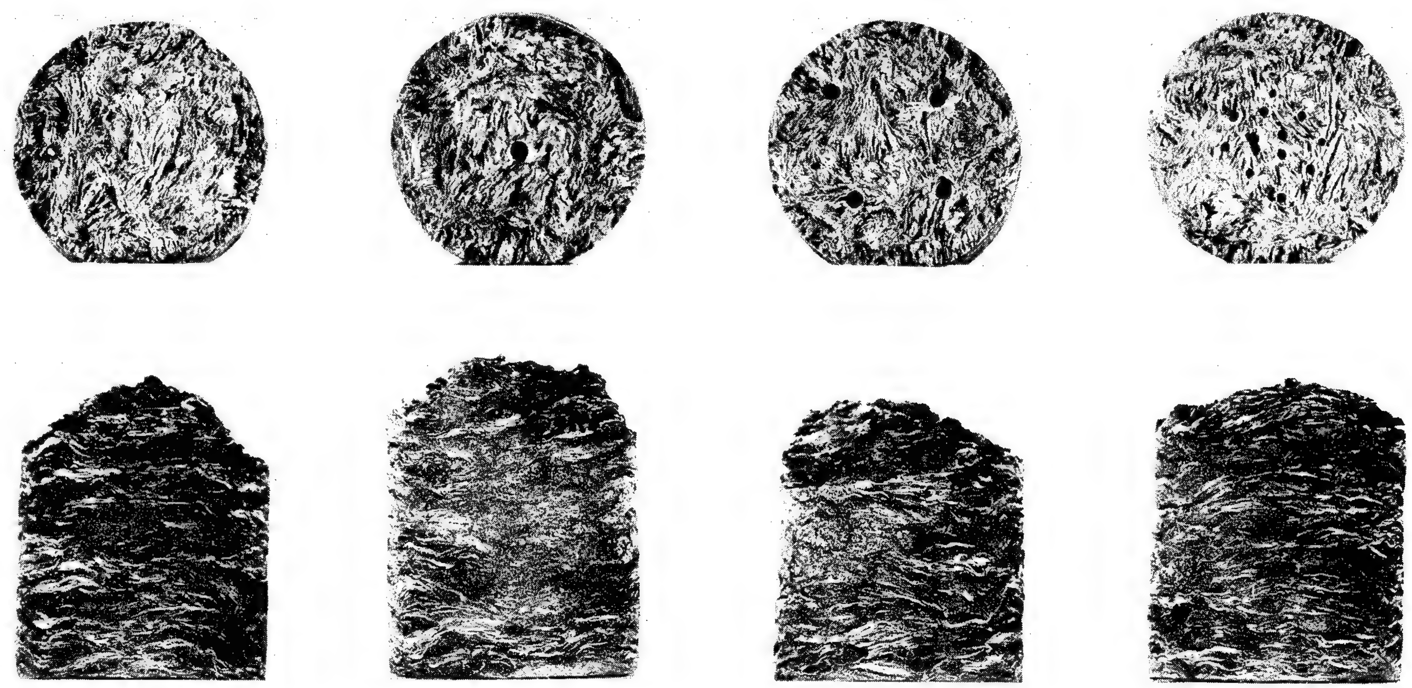

No holes | 1 hole | 4 holes | 13 holes

L-70-4714

Figure 15.- Photographs of models (after testing) showing the effect of hole patterns in the material at the highest pressure test condition. $p_s = 11$ atm; $K_o = 0.10$; $\dot{q}_s = 610$ Btu/ft^2-sec (6.93 MW/m^2); $H_s = 1100$ Btu/lbm (2.55 MJ/kg); $t = 20.0$ seconds.

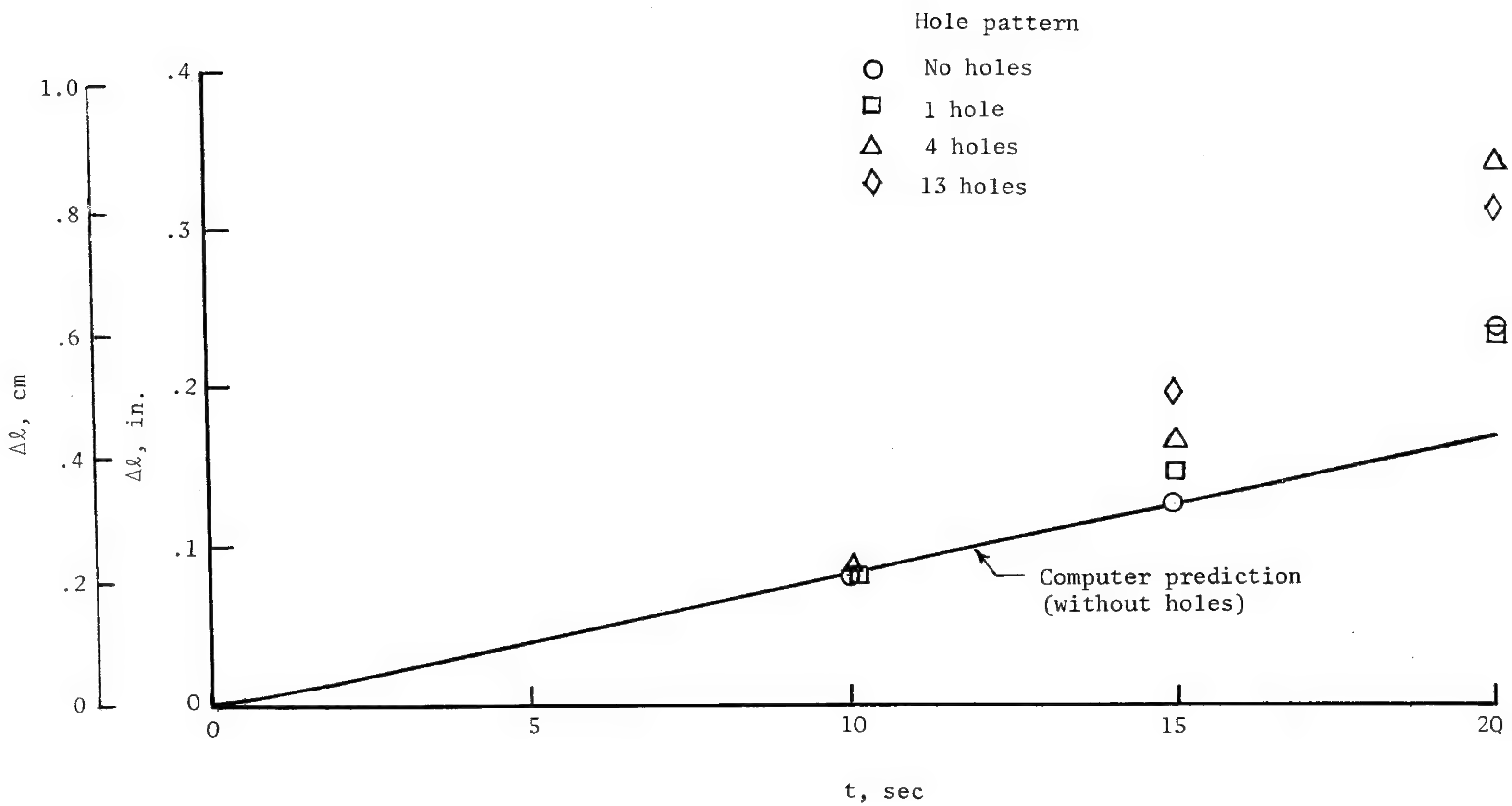

Figure 16.- The stagnation-point recession for the models with hole patterns at the highest pressure test condition. $p_s = 11$ atm; $K_o = 0.10$; $\dot{q}_s = 610$ Btu/ft^2-sec (6.95 MW/m^2); $H_s = 1100$ Btu/lbm (2.55 MJ/kg).

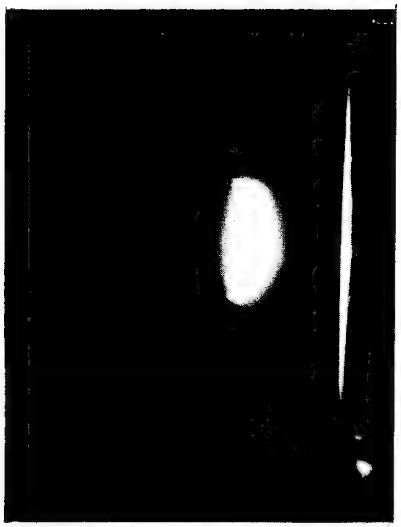

Between water pulses

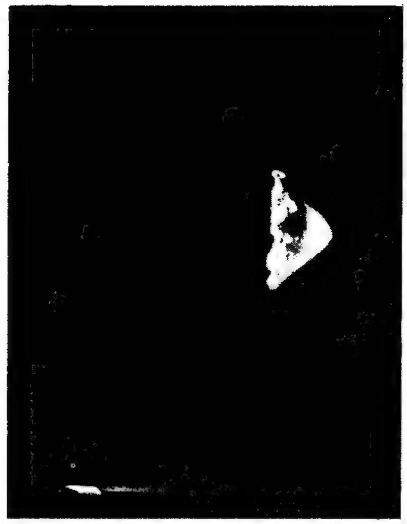

During a water pulse
$\dot{w}$=.059 lbm/sec (.027 kg/s)

(a) Stagnation-point injection.

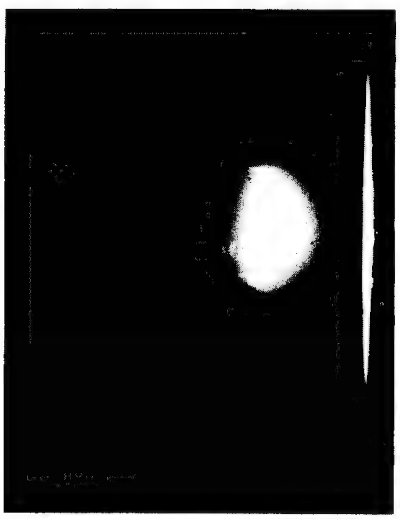

Between water pulses

During a water pulse
$\dot{w}$=.135 lbm/sec (.061 kg/s)

L-70-4715

(b) Side-wall injection.

Figure 17.- Photographs of the water-injection models during a test at the high-pressure test condition. p_s = 11 atm; K_o = 0.10; $\dot{q}_s$ = 610 Btu/ft^2-sec (6.95 MW/m^2); H_s = 1100 Btu/lbm (2.55 MJ/kg).

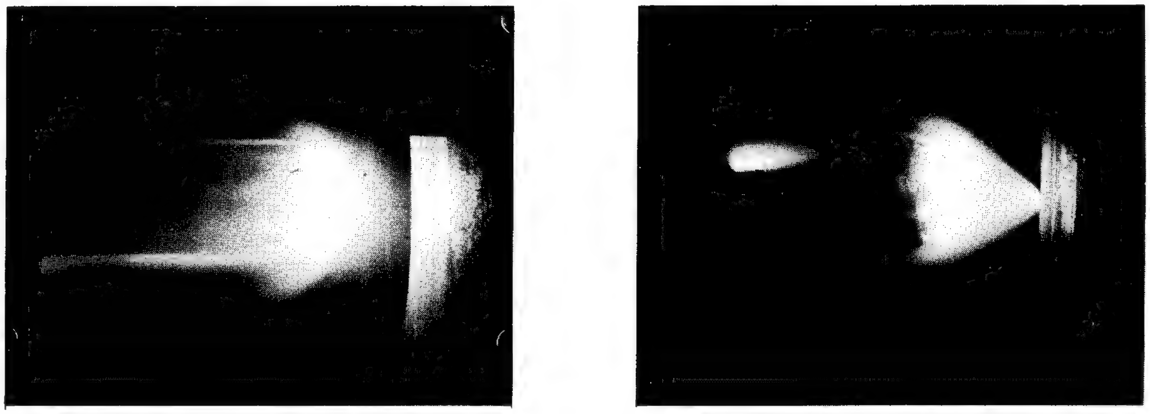

Between water pulses

During a water pulse
$\dot{w}$=.024 lbm/sec (.011 kg/s)

(a) Stagnation-point injection.

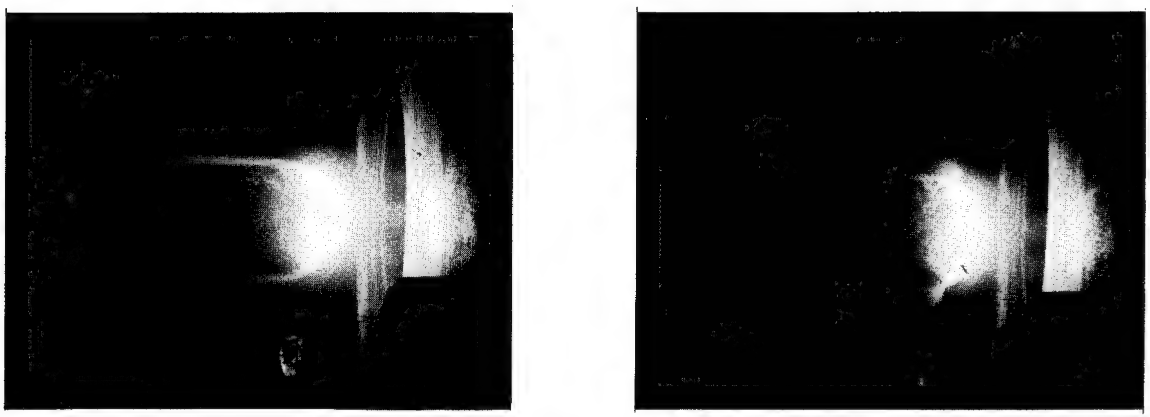

Between water pulses

During a water pulse
$\dot{w}$=.035 lbm/sec (.016 kg/s)

(b) Sidewall injection.

(b) Sidewall injection. L-70-4716

Figure 18.- Photographs of the water-injection models during a test at the low-pressure test condition. p_s = 0.60 atm; K_o = 0.232; $\dot{q}_s$ = 1600 Btu/ft^2-sec (18.2 MW/m^2); H_s = 11 000 Btu/lbm (25.5 MJ/kg).

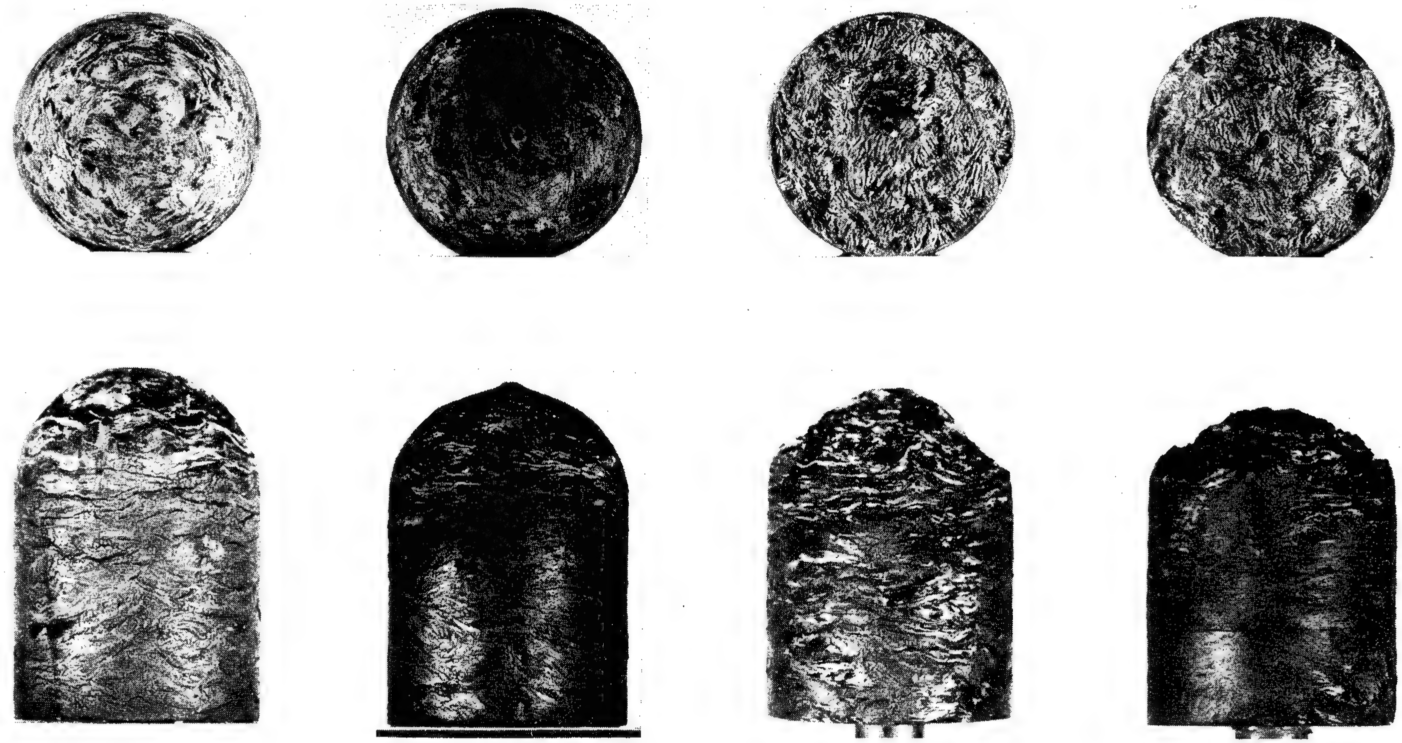

Stagnation-point injection | Sidewall injection | Stagnation-point injection | Sidewall injection

L-70-4717

(a) $p_s = 0.60$ atm; $K_o = 0.23$;
$\dot{q}_s = 1600$ Btu/ft^2-sec (18.20 MW/m^2);
$H_s = 11\ 000$ Btu/lbm (25.50 MJ/kg);
$t = 5.0$ seconds.

(b) $p_s = 11.00$ atm; $K_o = 0.10$.
$\dot{q}_s = 610$ Btu/ft^2-sec (6.93 MW/m^2);
$H_s = 1100$ Btu/lbm (2.55 MJ/kg);
$t = 10.0$ seconds.

Figure 19.- Photographs of the water-injection models (after testing) from both the low-pressure and the high-pressure test conditions.

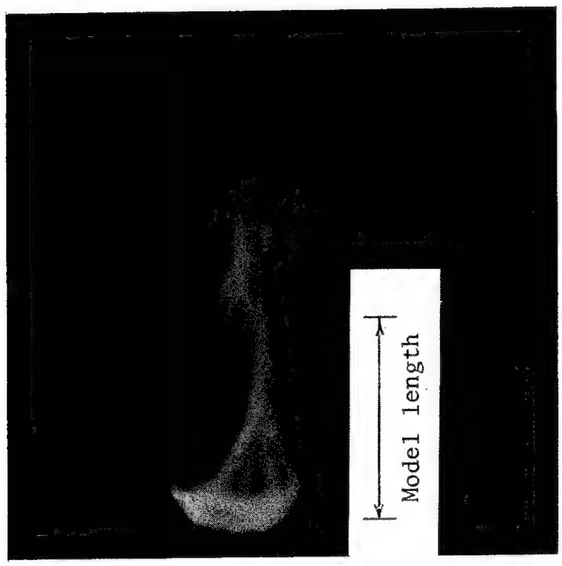

L-70-4718

Figure 20.- Photograph showing flaming of the model after retraction from stream in the 11-inch ceramic-heated tunnel.

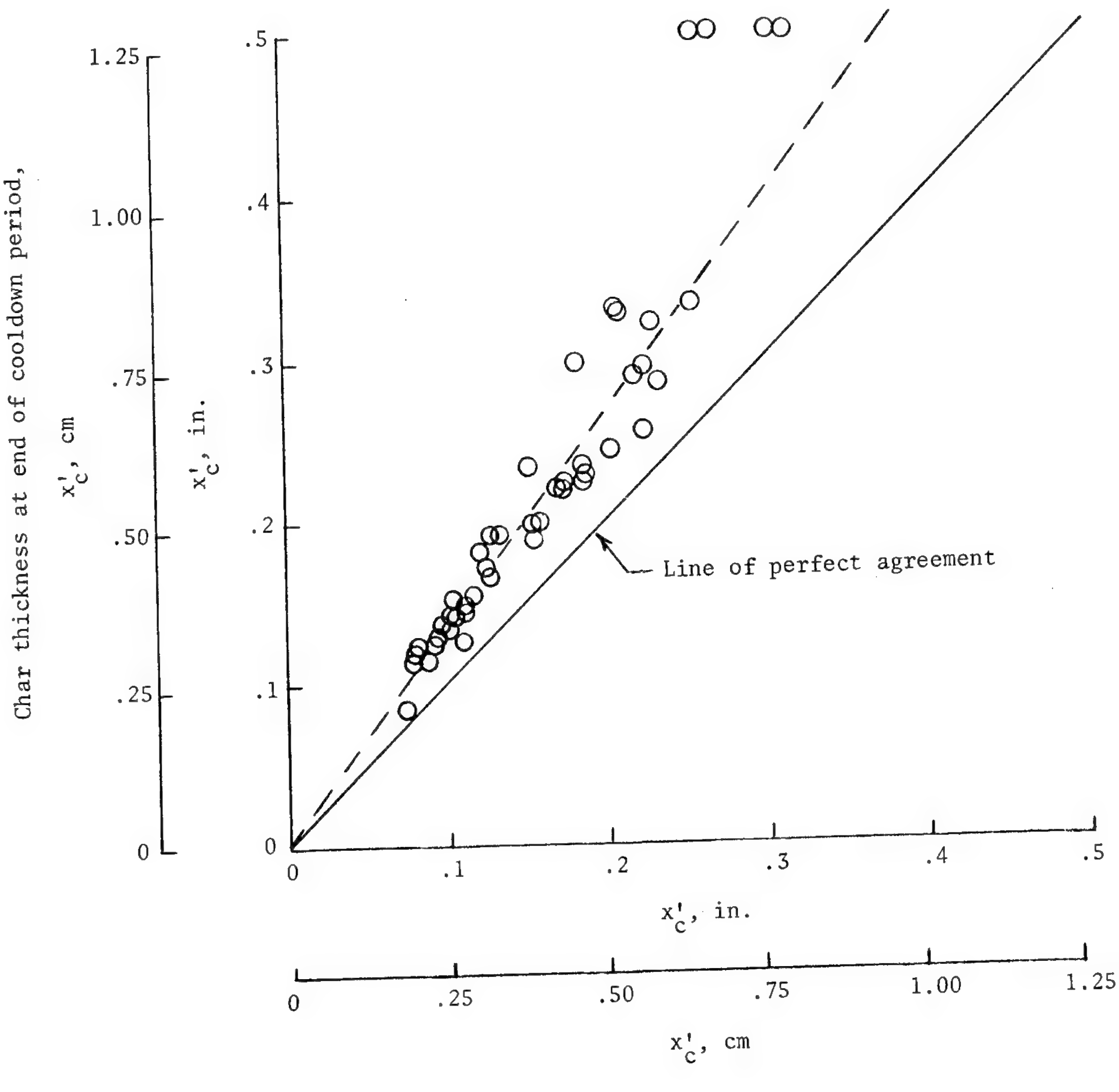

Figure 21.- The comparison from computer predictions of the stagnation-point char thicknesses at the end of model exposure time and at the end of the cooldown period.

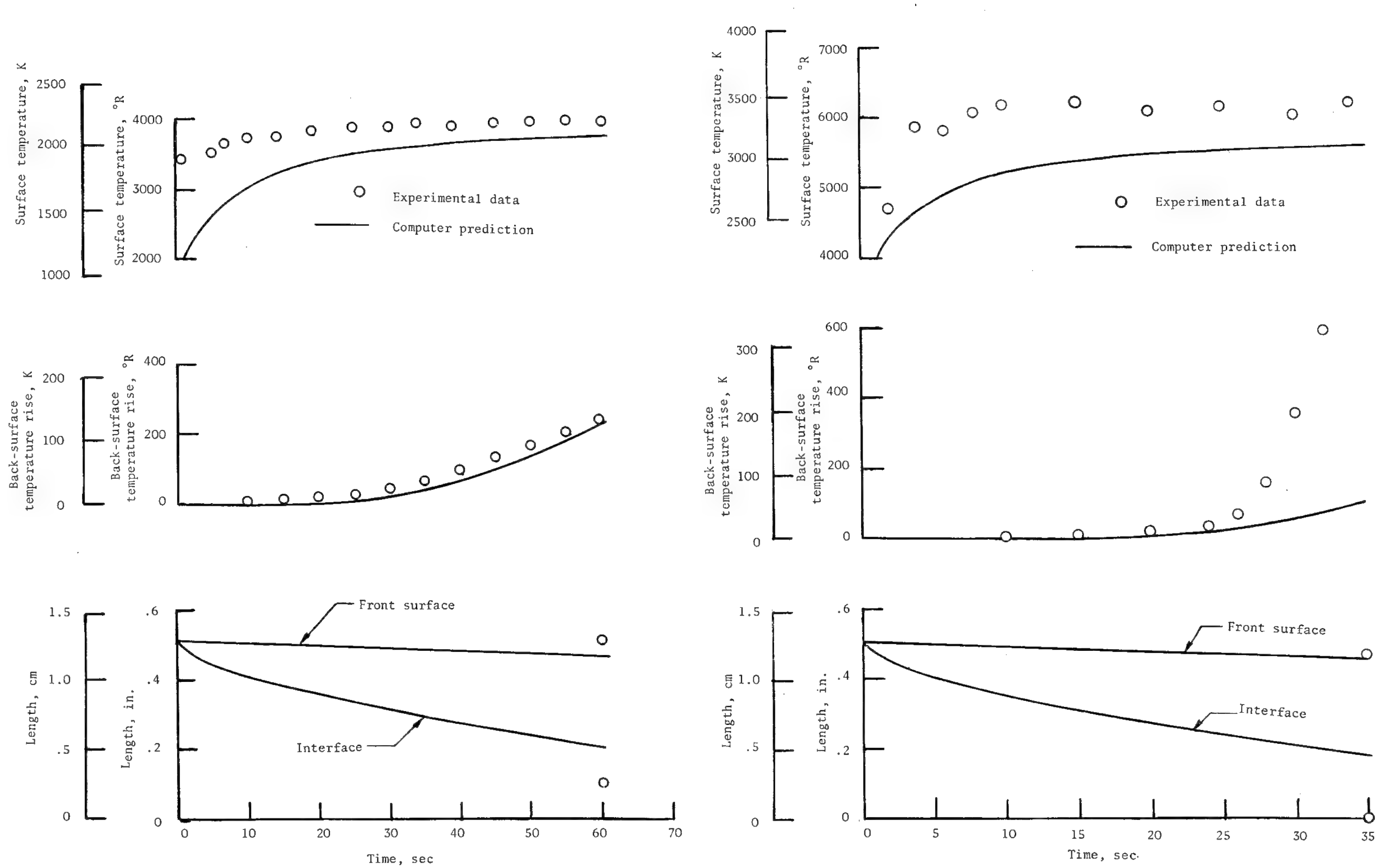

(a) $p_s = 0.07$ atm; $K_o = 0.23$;
$\dot{q}_s = 128$ Btu/ft^2-sec (1.44 MW/m^2);
$H_s = 5000$ Btu/lbm (11.60 MJ/kg).

(b) $p_s = 0.32$ atm; $K_o = 0.23$.
$\dot{q}_s = 621$ Btu/ft^2-sec (7.05 MW/m^2);
$H_s = 11\ 500$ Btu/lbm (26.65 MJ/kg).

Figure 22.- Typical comparisons between experimental results and computer predictions for model design shown in figure 7.

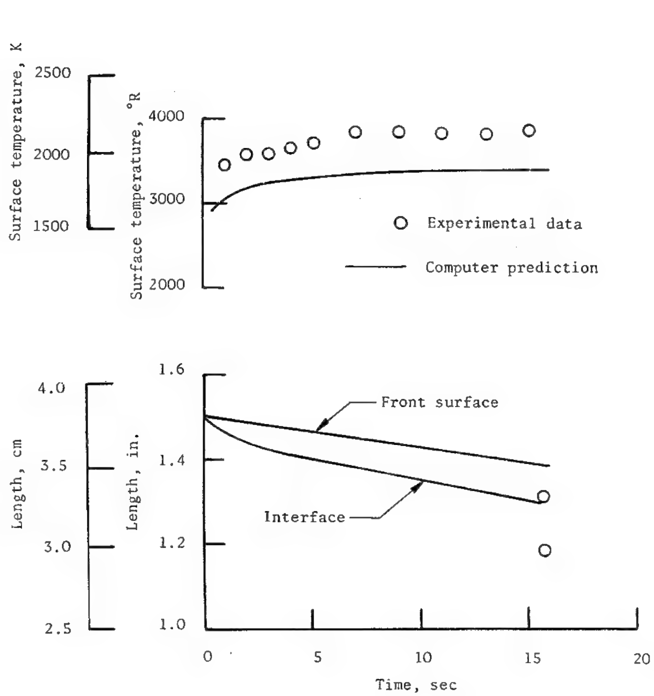

(a) $p_s = 10.91$ atm; $K_o = 0.09$;
$\dot{q}_s = 426$ Btu/ft^2-sec (4.84 MW/m^2);
$H_s = 822$ Btu/lbm (1.91 MJ/kg).

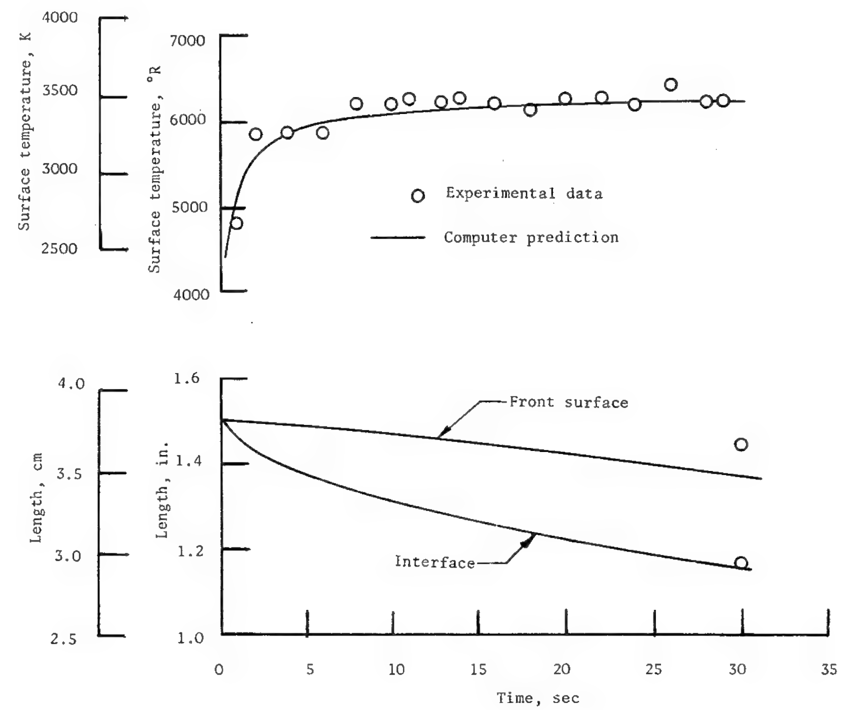

(b) $p_s = 0.31$ atm; $K_o = 0.23$;
$\dot{q}_s = 1250$ Btu/ft^2-sec (14.20 MW/m^2);
$H_s = 10\,800$ Btu/lbm (25.05 MJ/kg).

Figure 23.- Typical comparisons between experimental results and computer predictions for model design shown in figure 3(a).

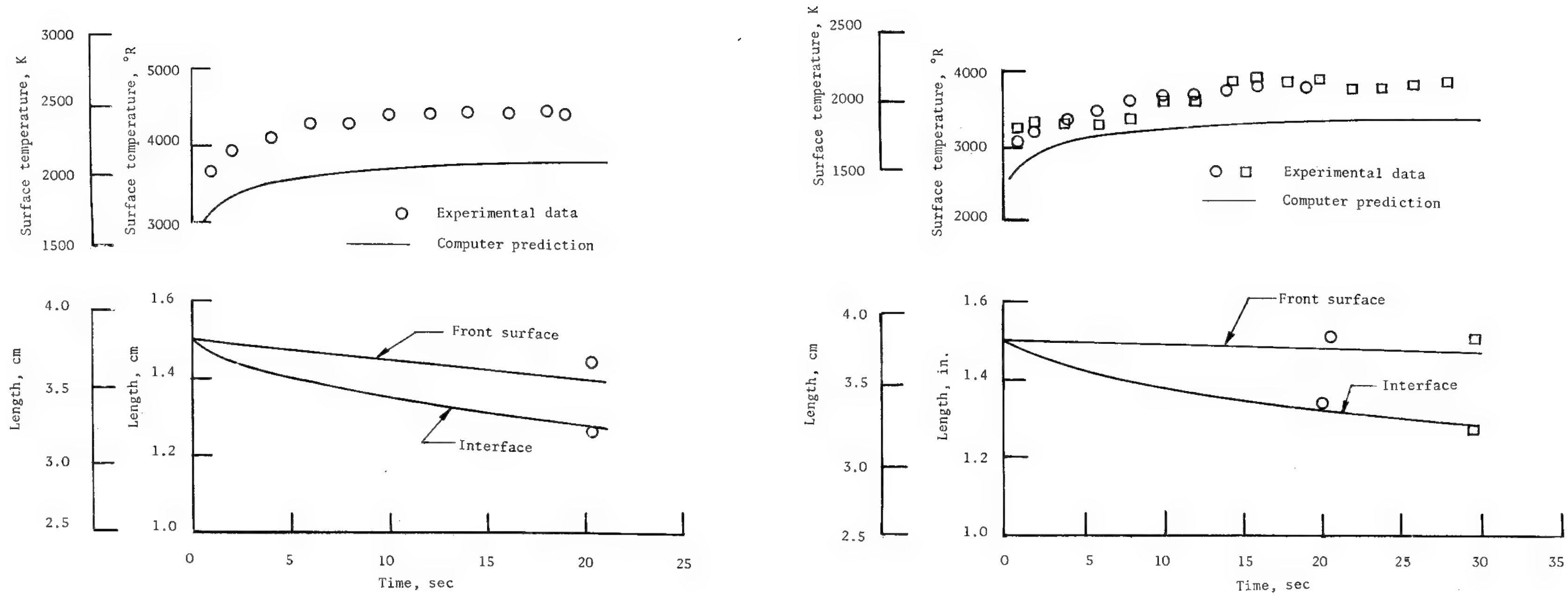

(a) p_s = 5.88 atm; K_o = 0.13;
$\dot{q}_s$ = 302 Btu/ft^2-sec (3.43 MW/m^2);
H_s = 1100 Btu/lbm (2.55 MJ/kg).

(b) p_s = 4.97 atm; K_o = 0.02;
q_s = 304 Btu/ft^2-sec (3.45 MW/m^2);
H_s = 1100 Btu/lbm (2.55 MJ/kg).

Figure 24.- Typical comparisons between experimental results and computer predictions for model design shown in figure 3(b).

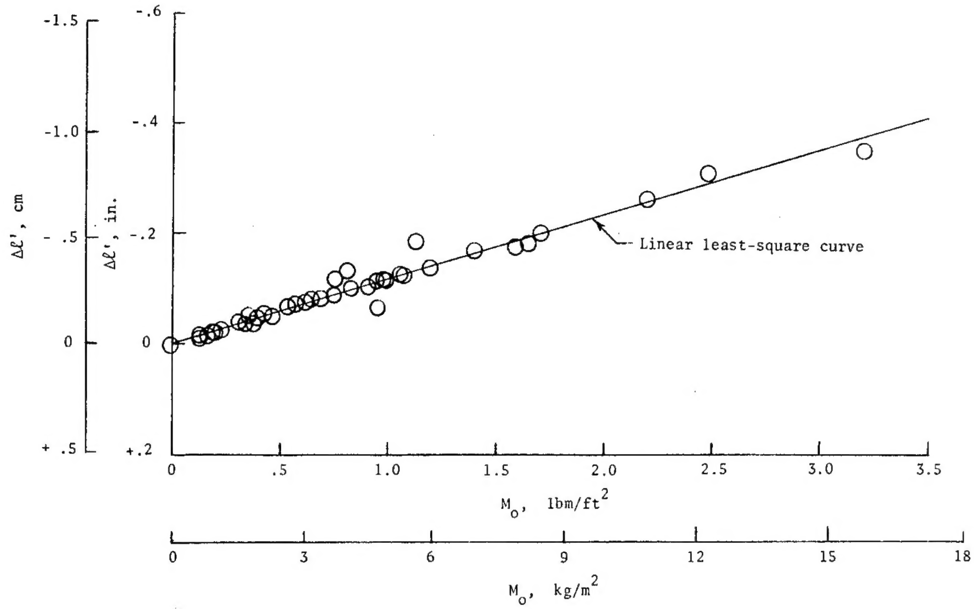

(a) Results from computer predictions.

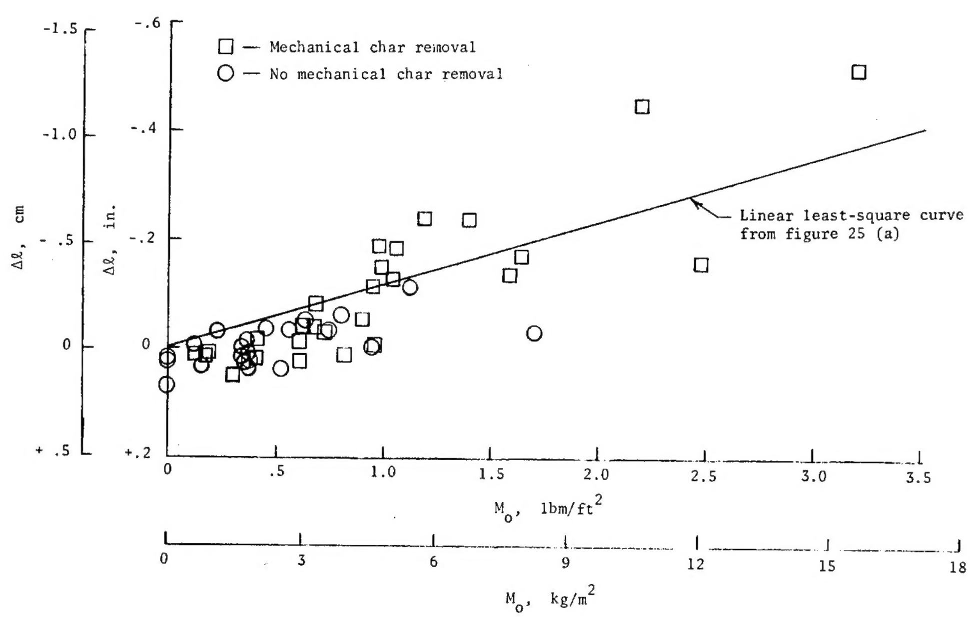

(b) Results from experimental data.

Figure 25.- Comparison between the experimental results and the computer predictions of model stagnation-point length change as a function of total cold-wall oxygen mass flux. The linear least-square curve is based on the results from the computer predictions.

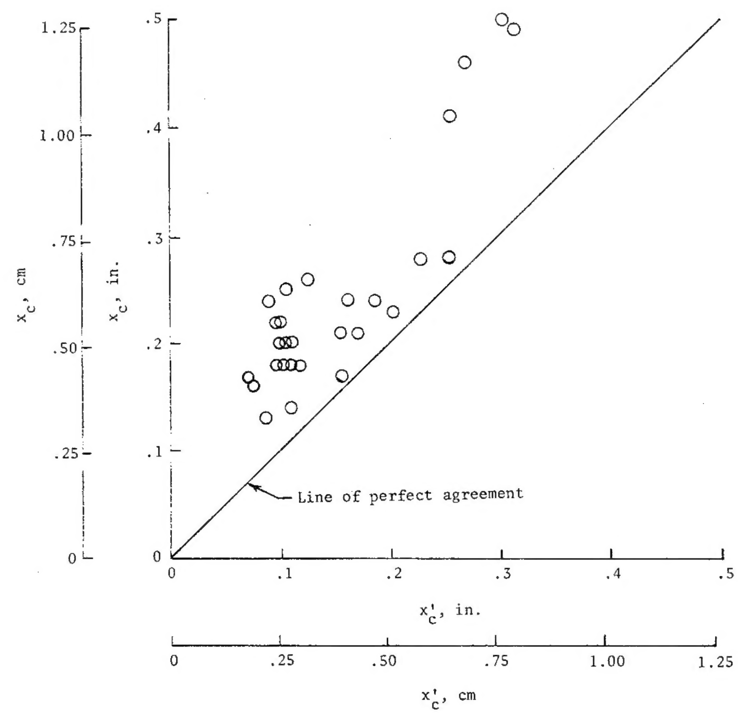

(a) Computer predictions for end of model exposure time.

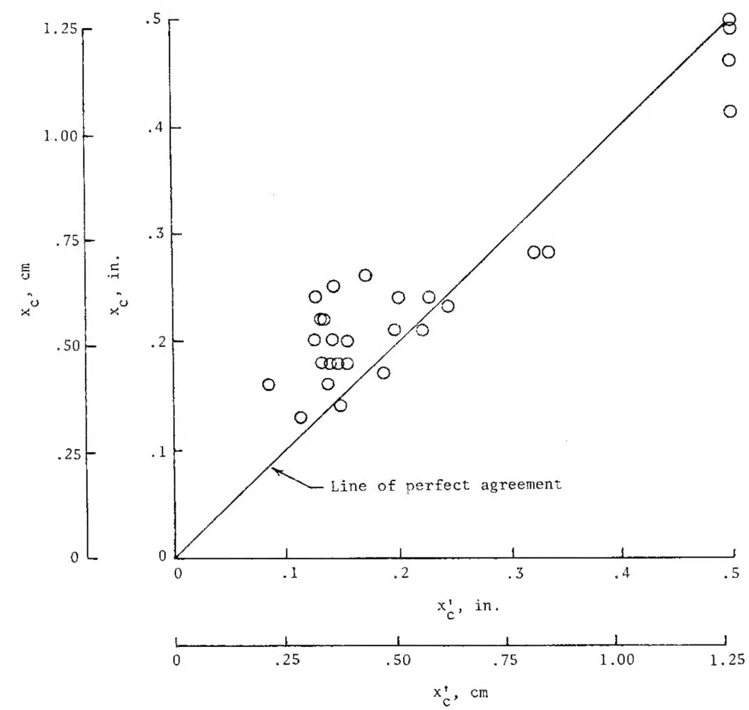

(b) Computer predictions for end of cooldown period.

Figure 26.- The comparisons between the experimental data and the computer predictions for the stagnation-point char thicknesses.

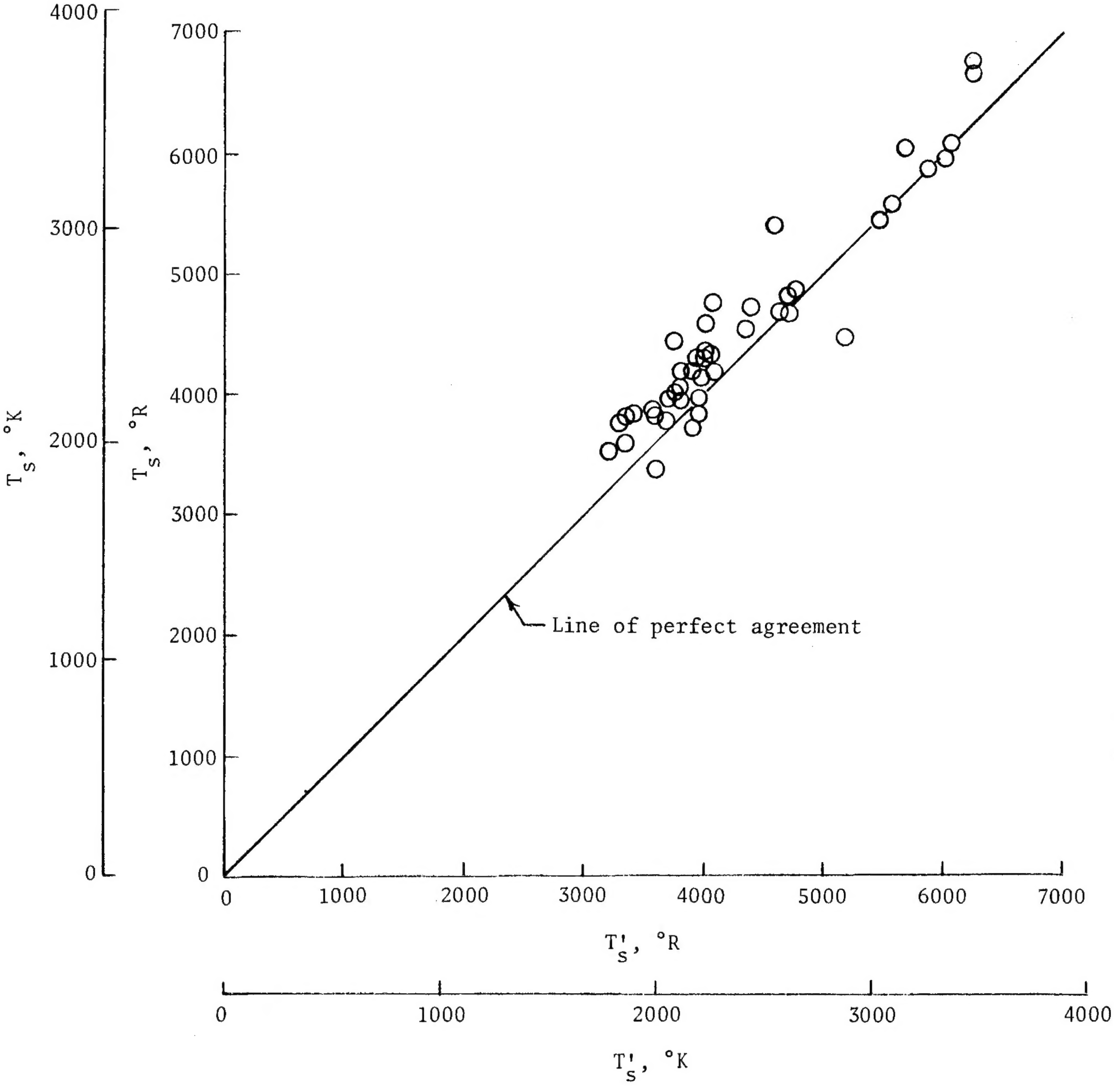

Figure 27.- The comparison between the experimental data and the computer predictions for the model stagnation-point surface temperature.

NATIONAL AERONAUTICS AND SPACE ADMINISTRATION
WASHINGTON, D. C. 20546

OFFICIAL BUSINESS

FIRST CLASS MAIL

POSTAGE AND FEES PAID
NATIONAL AERONAUTICS AND
SPACE ADMINISTRATION

03U 001 43 50 3DS 7C240 00942
PICATINNY ARSENAL
PLASTICS TECHNICAL EVALUATION CENTER
DOVER, NEW JERSEY 07801

ATT SMUPA-VP3 3 Y C/

POSTMASTER: If Undeliverable (Section 158 Postal Manual) Do Not Return

"The aeronautical and space activities of the United States shall be conducted so as to contribute . . . to the expansion of human knowledge of phenomena in the atmosphere and space. The Administration shall provide for the widest practicable and appropriate dissemination of information concerning its activities and the results thereof."

— NATIONAL AERONAUTICS AND SPACE ACT OF 1958

NASA SCIENTIFIC AND TECHNICAL PUBLICATIONS

TECHNICAL REPORTS: Scientific and technical information considered important, complete, and a lasting contribution to existing knowledge.

TECHNICAL NOTES: Information less broad in scope but nevertheless of importance as a contribution to existing knowledge.

TECHNICAL MEMORANDUMS: Information receiving limited distribution because of preliminary data, security classification, or other reasons.

CONTRACTOR REPORTS: Scientific and technical information generated under a NASA contract or grant and considered an important contribution to existing knowledge.

TECHNICAL TRANSLATIONS: Information published in a foreign language considered to merit NASA distribution in English.

SPECIAL PUBLICATIONS: Information derived from or of value to NASA activities. Publications include conference proceedings, monographs, data compilations, handbooks, sourcebooks, and special bibliographies.

TECHNOLOGY UTILIZATION PUBLICATIONS: Information on technology used by NASA that may be of particular interest in commercial and other non-aerospace applications. Publications include Tech Briefs, Technology Utilization Reports and Notes, and Technology Surveys.

Details on the availability of these publications may be obtained from:

SCIENTIFIC AND TECHNICAL INFORMATION DIVISION
NATIONAL AERONAUTICS AND SPACE ADMINISTRATION
Washington, D.C. 20546